Neurodegeneration impairs the consolidation of developmentally synchronized behavioral patterns

Lior Laufer[1], Sharon Inberg[1], Eshkar Nir, Adi Sufrin, and Shay Stern[2]

Faculty of Biology, Technion- Israel Institute of Technology, Haifa, Israel

[1] These authors contributed equally
[2] Lead contact

Correspondence: sstern@technion.ac.il

Abstract

Animals generate predictable patterns of behavior that are robustly synchronized with the developmental clock. However, the long-term establishment of time-locked behaviors across development, and the neuronal alterations that may impair them, remain underexplored. Here, by quantifying the temporal synchronization of behavior in multiple isolated *C. elegans* individuals throughout their complete development time, we show that robust behavioral synchronization consolidates across stages as development progresses. Analyses of multiple mutant populations with perturbed neuronal function or structure reveal that neurodegeneration in specific circuits impairs the developmental organization of behavior. In one of the cases, protection from neurodegeneration of the circuit of touch receptor neurons restored normal modes of long-term behavior. Moreover, at the neuronal activity level, we found altered activity patterns in downstream motor neurons following neurodegeneration. These results suggest the impairment of developmental patterns of synchronized behavior by localized neurodegenerative processes within the nervous system.

Introduction

Individuals exhibit patterns of behavior over long timescales that are temporally synchronized. For example, activity and sleep cycles are regulated by a circadian rhythm across species (Konopka and Benzer, 1971; Panda et al., 2002). In addition, the lunar cycle affects the foraging of fruit bats and kangaroo rats (Daly et al., 1992; Morrison, 1978), while circannual rhythms control bird migration (Gwinner, 1986) and hibernation cycles in chipmunks (Kondo et al., 2006). In particular, during development, animals display long-term temporal changes in behavior that depend on the specific developmental window and are synchronized with the developmental clock of each individual. For instance, *Drosophila melanogaster* shows a 'foraging' state during the third-instar larvae and a 'wandering' state during the pre-pupation stage (Sokolowski et al., 1984). In addition, behavioral patterns in honeybees are modified over their lifetime (Vance et al., 2009), and startle response in fish is shaped throughout development (Kimmel et al., 1974). Moreover, fear extinction learning in both humans and mice is altered at specific developmental windows (Pattwell et al., 2012).

C. elegans is an efficient model system for studying the temporal organization of behavior across developmental timescales due to its short development time of 2.5 days, genetically homogenous population, and the well-defined structure of its nervous system (White et al., 1986). It was previously demonstrated that isolated *C. elegans* individuals show stereotyped long-term patterns of behavior that are highly dynamic throughout development (Stern et al., 2017; Harel et al., 2024). However, it is still unclear how behavioral synchronization with the developmental clock is continuously established across and within distinct developmental stages, and which impairments within the nervous system may lead to alterations in this robust behavioral synchronization.

The function of the nervous system can be shaped by the modification of neuronal states, as well as by structural changes within the nervous system during development or adulthood. In *C. elegans*, both naturally occurring programmed cell death via apoptosis (Ellis and Horvitz, 1986) or neurodegeneration via cellular necrosis (Chalfie and Wolinsky, 1990; Driscoll and Chalfie, 1991; Treinin and Chalfie, 1995) were shown to modify the nervous system structure during its formation. While

neurodegeneration has been linked to behavioral alterations during specific developmental windows, it is currently unclear what are the continuous effects of these neurodegenerative processes across all developmental stages on long-term behavioral patterns and their temporal synchronization. Here, by monitoring the long-term locomotory behaviors of multiple isolated *C. elegans* individuals across their full development time and quantifying their temporal behavioral synchronization across distinct developmental stages, we found a gradual consolidation of temporal behavioral synchronization as development progresses. We further revealed that within multiple mutant populations for neuronal genes that affect both the neuromodulatory state of the nervous system, as well as its structure, the level of developmental synchronization of behavior was modified in a stage-specific manner. Specifically, we found that degenerins-induced neurodegenerative processes in specific circuits strongly impair the temporal synchronization across development and that neuroprotection from circuit degeneration can reestablish normal modes of long-term behavior. Interestingly, in one of the cases, we further revealed alteration in the activity patterns of multiple downstream motor neurons in individuals in which the localized circuit of touch receptor neurons is degenerated. Overall, these results shed light on the establishment of robust behavioral synchronization throughout development time and the impairment of developmental patterns of behavior by the neurodegeneration of localized circuits.

Results

C. elegans shows consolidation of behavioral time-synchronization throughout development

To study the temporal organization of behavior across development at the individual and population level, we utilized long-term behavioral monitoring of multiple individuals across their complete developmental trajectory (Stern et al., 2017; Harel et al., 2024). In particular, in this imaging system, the behavior of single isolated individuals is continuously tracked from egg hatching to 16 hours of adulthood (~2.5 days) in custom-made multi-well plates, at high spatiotemporal resolution (3 fps, ~10 μm) and under a tightly controlled environment (Fig. 1A). Wild-type individuals show variation in their development time (±5%) (Fig. S1A). To align behavioral trajectories of different

individuals we divided the developmental stage of each single individual into 75 time windows (Fig. S1B) (Stern et al., 2017; Ali Nasser et al., 2023). While growing in a food environment, *C. elegans* shifts between active and inactive locomotory states that last seconds to minutes, called roaming and dwelling (Ben Arous et al., 2009; Flavell et al., 2013; Fujiwara et al., 2002; Stern et al., 2017). It was previously shown that during development, individuals show long-term patterns of roaming and dwelling behavior that are highly dynamic across and within stages (Fig. 1B,D; Fig. S1C,D) (Stern et al., 2017). These long-term behavioral patterns are manifested by specific developmental periods of high roaming activity, such as during the first half of the L2, L3, and L4 larval stages, as well as peaks of roaming that are more limited in time, such as during the end of the L4 stage. These stereotyped temporal patterns of behavior shown among isolated individuals suggest that specific behavioral outputs in *C. elegans* are predictable in time and temporally synchronized with the developmental clock of each single individual. To systematically study the behavioral synchronization, and how it is established as development progresses, we quantified the behavioral time-correlation among wild-type individuals at distinct developmental stages. High behavioral time-correlations would indicate that different individuals within the population tend to show similar structures of roaming activity patterns across developmental windows, indicating the robust synchronization of long-term behavior with the time of development (Fig. 1C; Fig. S1E). In contrast, low time-correlations would indicate that the behavioral structure of different individuals is variable in time (up to randomness), suggesting a low level of robustness in forming predictable patterns of behavior during specific developmental windows (Fig. 1C; Fig. S1E). By first quantifying the temporal synchronization among wild-type individuals across their complete developmental trajectory, we found that overall, individuals showed higher behavioral synchronization over time, compared to a randomly shuffled dataset (Fig. S1F). Next, to further study whether the levels of developmental time-synchronization change across distinct developmental stages, we separately analyzed time-correlations among individuals within each of the five developmental stages (L1 to L4 and adulthood). Interestingly, we found that the robustness of developmental time-synchronization increased across larval stages (Fig. 1D,E). In particular, during the L1 stage, individuals showed patterns of roaming activity

that are disorganized in time, reflected by the close-to-random correlations during this stage. Following the transition to the L2 stage, individuals showed significantly higher temporal synchronization, which gradually increased during the L3 and L4 stages (Fig. 1D,E). After the transition to adulthood, animals showed a slight decrease in temporal correlations, that were still significantly higher than in the early L1 stage. This relative strengthening of behavioral time-correlations across development time represents a 'consolidation' of developmental synchronization of behavior (Fig. 1E). These results reveal the dynamics of establishment of time-synchronized behavior during *C. elegans* development.

Analysis of consistent and stage-specific effects on behavioral time-synchronization in multiple neuronal gene mutants

To reveal underlying neuronal processes that may affect the time-locked behavioral patterns across and within developmental stages, we performed a candidate genetic screen to identify mutants in which the developmental synchronization of behavior among individuals is altered. In particular, we systematically analyzed the temporal behavioral synchronization within 13 populations mutant for various neuronal genes that are involved in neuromodulation, sensation, epigenetic modifications, and changes in the nervous system structure by necrotic degeneration or apoptosis (Fig. 2A; Fig. S3A). For each mutant population, we quantified the temporal correlations in each of the developmental stages and compared them to the wild-type population. These analyses revealed multiple effects on the behavioral time-synchronization during development that may be systematic across most of the developmental trajectory or exposed at specific developmental stages. For instance, individuals mutant for the epigenetic modifiers *met-2* (Andersen and Horvitz, 2007) and *hpl-1* (Couteau et al., 2002) that are expressed within neurons (Taylor et al., 2021) showed lower levels of behavioral time-synchronization across multiple developmental stages (L2-Adult), compared to the wild-type population (Fig. 2A-E; Fig. S2A). Similarly, mutants for *npr-1* neuropeptide receptor which were previously measured for their long-term roaming activity across development (Stern et al., 2017; Harel et al., 2024), showed a significant decrease in the temporal synchronization among individuals during the L3-Adult

developmental stages, but a strong increase in behavioral synchronization during the L1 stage (Fig. 2A-C,F; Fig. S2A). In contrast to the identified stage-specific decrease in behavioral time-synchronization, we also found that in a fraction of the mutant populations the behavioral time-synchronization across development was increased across most of the developmental stages. For example, mutants for the *osm-9* channel involved in sensation of environmental inputs (Colbert et al., 1997) and *tph-1* serotonin-deficient individuals showed significantly higher temporal correlations compared to the wild-type population during most of the developmental stages (Fig. 2A-C,G; Fig. S2B,D). Interestingly, some of the effects on the temporal synchronization were much more limited in time, as *tax-4* mutant individuals that are sensory-defective (Bargmann et al., 1993; Dusenbery et al., 1975; Mori and Ohshima, 1995) showed higher levels of behavioral time synchronization during the L2 stage (Fig. 2A-C,H; Fig. S2B,D).

While we were able to detect strong effects on the temporal behavioral synchronization in some of the mutant populations, other populations showed milder effects on behavioral time-synchronization. In particular, we found that populations mutant for the *cat-2*, and *tdc-1* genes required for the production of specific neuromodulators (dopamine and tyramine/octopamine, respectively), as well as individuals mutant for the glutamate receptor *glr-1* and the apoptotic *ced-3* gene in which the number of neurons is increased, all showed lower levels of impairment of the behavioral time synchronization (Fig. 2A-C; Fig. S2C,E-H). Overall, these results reveal specific neuronal genes that affect the robustness of temporal synchronization of long-term behavioral patterns across distinct developmental stages.

Degeneration of specific neuronal circuits impairs developmental patterns of behavior

To further study the effects of specific alterations to the nervous system structure on the temporal behavioral patterns across development, we have monitored multiple neurodegenerative mutants in which hyperactive forms of the degenerins *deg-1*, *deg-3,* and *mec-4* lead to cell-autonomous necrotic degeneration of specific neuronal circuits (Chalfie and Wolinsky, 1990; Driscoll and Chalfie, 1991; Treinin and Chalfie, 1995). Surprisingly, we found that all three *deg-1*, *deg-3*, and *mec-4* neurodegenerative mutant

populations showed significant impairment of the temporal correlations of behavior, compared to wild-type (Fig. 2A-B; Fig. 3; Fig. S3B-D). In particular, the *deg-1* and *mec-4* genes encode subunits of sodium ion channels involved in mechano-sensation (Chalfie and Sulston, 1981; Cueva et al., 2007; Geffeney et al., 2011; O'Hagan et al., 2005; Suzuki et al., 2003). The localization of hyperactive forms of these channels to specific neuronal circuits may generate an imbalance of ion flow (Bianchi et al., 2004), causing cell death by necrosis during development.

The expression of the *deg-1* hyperactive channel leads to degeneration of a limited set of neurons including ASH, IL1, AVD, AVG, and PVC (Chalfie and Wolinsky, 1990; Hall et al., 1997). Analyses of behavioral time-synchronization in *deg-1* mutant individuals showed that behavioral time-synchronization throughout development time was strongly impaired, as temporal correlations were decreased during the L2-Adult stages (Fig. 3A,D).

Similarly, in hyperactive mutants for the *mec-4* channel, a highly localized circuit which is composed of only six touch receptor neurons is degenerated (pair of ALM, pair of PLM, AVM, PVM) (Driscoll and Chalfie, 1991). We found that the temporal structure of behavior across larval stages in these neurodegenerative mutants was strongly impaired. In particular, similar to the *deg-1* mutants, during the L2-L4 stages *mec-4* neurodegenerative mutants showed significantly lower time-correlation (Fig. 3B,E). Interestingly, during adulthood, the temporal synchronization was elevated in *mec-4* mutant individuals, suggesting that in *mec-4* neurodegenerative mutants the robustness of behavioral time synchronization may be affected during intermediate developmental stages. Furthermore, the analyzed hyperactive mutant forms of *deg-1* and *mec-4* of the degenerins were selected based on their known strong neurotoxic effect, which leads to neurodegeneration early in development (*deg-1(u38)* and *mec-4(u231)*) (Hall et al., 1997). Analysis of an additional *mec-4* hyperactive mutant allele in which neurodegeneration phenotypes appear later during larval stages (*mec-4(e1611))* (Hall et al., 1997), probably due to a milder neurotoxic effect, showed a strong disruption of the wild-type synchronized activity peaks, but also the generation of alternative short-term peaks (Fig. S3E,F).

In contrast to the degenerins *deg-1* and *mec-4* which encode sodium ion channels, the gene *deg-3* encodes a subunit of a nicotinic acetylcholine receptor (Treinin and Chalfie, 1995). The hyperactive form of *deg-3* leads to similar necrotic degeneration in a larger group of neurons overlapping with those of *deg-1* and *mec-4* (including PLM, PVC, PVD, PVM, ALM, AVM, AVG and IL1). Similar to *deg-1* and *mec-4* neurodegenerative mutants, analysis of long-term behavior throughout development in *deg-3* neurodegenerative mutants revealed modifications in the temporal behavioral patterns during multiple developmental stages (L2-L4 larval stages) (Fig. 3C,F). In summary, these results suggest that neuronal degeneration of localized neuronal circuits within the nervous system by different molecular pathways alters developmental patterns of long-term behavior.

Protection from degeneration of the TRN circuit reestablishes normal modes of long-term behavior across development

As we detected the impairment of long-term behavior across developmental stages in multiple neurodegenerative mutants (Fig. 3, Fig. S3), we next focused on studying the effects of neuroprotection from degeneration in one of these cases, in which the hyperactive form of *mec-4* generates a relatively limited degeneration in the six touch receptor neurons (TRN) (Driscoll and Chalfie, 1991). Specifically, we asked whether neuroprotection from degeneration would reestablish normal temporal patterns of behavior across developmental stages (Fig. 4A). We initially tested whether the degeneration of *mec-4* expressing neurons in the TRN circuit is required for the impairment of temporal behavioral structures, or whether the loss of function of the MEC-4 mechanosensory channel within these neurons is sufficient to produce the same effect. To study this, we measured the behavior of two loss-of-function mutant alleles of the *mec-4* gene which impair the function of the MEC-4 channel without causing neurodegeneration of the TRN circuit. We found that in contrast to the *mec-4* neurodegenerative mutants, the loss-of-function *mec-4* mutants did not show the decrease in the temporal synchronization of behavioral structures during development (Fig. 4B,E; Fig. S4A-D,G-H). In addition, we found that inhibition of the TRN neuronal activity by the cell-specific expression of HisCl (Pokala et al., 2014) showed only minor

effects on the temporal behavioral patterns (Fig. S4K). These results suggest that degeneration of the TRN circuit and not the impairment of MEC-4 itself is required for the alteration of the temporal behavioral patterns.

Next, we further asked whether preventing the TRN neurodegeneration by using the drug amiloride, a known blocker of degenerin sodium channels (Bianchi et al., 2004; Brown et al., 2007; Goodman et al., 2002), would restore the normal behavioral patterns across development. We found that supplementing exogenous amiloride to the *mec-4* neurodegenerative mutant individuals which normally show the impairment of temporal behavioral structure, led to the rescue of the wild-type behavioral modes across developmental stages (Fig. 4C,F; Fig. S4E,I). These results imply that protection from degeneration by an external drug is sufficient for reestablishment of the normal developmental patterns of behavior. Furthermore, it has been previously shown that mutation of the calmodulin *crt-1* which is involved in homeostasis of cellular calcium reservoir from the ER genetically rescues the neurotoxic effect in *mec-4* neurodegenerative mutants (Xu et al., 2001). In contrast to *mec-4* limited expression in the nervous system, *crt-1* is broadly expressed across many neurons (Park et al., 2001; Taylor et al., 2021) and *crt-1* single mutants showed an additional synchronized roaming activity peaks at the end of each larval stage (Fig. S4J). We found that in *crt-1;mec-4* double mutants the temporal behavioral impairment generated by the *mec-4* neurodegeneration is eliminated (Fig. 4D,G; Fig. S4F). As expected, the additional synchronized activity peaks detected in the *crt-1* single mutants were also detected in the *crt-1*;mec-4 double mutants (Fig. S4J), suggesting an independent behavioral effect of *crt-1* during development, probably resulting from its much broader expression within the nervous system. Overall, these results show that TRN neurodegeneration is required for the impairment of long-term behavioral patterns and that protection from neurodegeneration of the TRN circuit restores temporal patterns of behavior across stages.

Neurodegeneration of the TRN circuit alters downstream neuronal activity dynamics in motor neurons

In addition to studying the long-term effects that are established at the behavioral level by the neurodegeneration of the TRN circuit, we sought to further test the effects of the TRN degeneration on the underlying neuronal activity patterns. In particular, we explored the possibility that the degeneration of the relatively small TRN circuit could lead to a more global modification of activity patterns in other neurons. To test the effects of TRN neurodegeneration on a large set of downstream neurons we analyzed the activity patterns of tens of ventral nerve cord (VNC) motor neurons by quantifying their calcium dynamics in the *mec-4* neurodegenerative mutant, as well as in the wild-type population in which the TRN circuit is intact (Fig. 5A; Fig. S5A). As most of the VNC motor neurons are born post-embryonically (Sulston and Horvitz, 1977; Von Stetina et al., 2005; Mulcahy et al., 2022), we hypothesized that they could be potentially affected by early onset of degeneration processes within the nervous system. In L4 wild-type individuals, where the TRN circuit is intact, VNC motor neurons showed relatively slow neuronal activity dynamics (average duration of activity bouts: ~0.85 min). In addition, the temporal pattern of spontaneous activity in different VNC motor neurons is highly correlated within the individual (Kato et al., 2015), and usually reflected by at least two groups of neurons that show opposite activity dynamics (Fig. 5B). By quantifying the neuronal activity of the VNC motor neurons in *mec-4* neurodegenerative L4 individuals we found that VNC neurons activity dynamics were impaired following neurodegeneration. In particular, neuronal alterations were reflected by the significantly higher amplitudes of neuronal activity during activity bouts in motor neurons (Fig. 5C) and longer durations of activity bouts in the neurodegenerative mutants (Fig. 5D). In contrast, the frequency of activity bouts over time was lower in the neurodegenerative mutants (Fig. 5E), compared to the wild-type. Moreover, similar profiles of neuronal alterations were evident across various types of the motor neurons (Fig. S5B). To ask if the altered states of the motor neurons are established earlier during development, we repeated our measurement in second larval stage (L2) individuals. Similar to L4 individuals, we found an increase in activity amplitudes and average duration of activity bouts also in younger L2 individuals (Fig. 5F-G; Fig. S5C). Interestingly, however, in contrast to L4 individuals the frequency of activity bouts in L2 individuals was similar to the wild-type populations (Fig. 5H), suggesting that specific

alterations of the neuronal activity dynamics in the neurodegenerative mutants are established later in development. These results suggest that neurodegeneration of a local circuit may modify the underlying activity patterns of other circuits within the nervous system, potentially by modifying information transfer within the network.

Discussion

Across different species, long-term behavioral patterns are highly structured across developmental timescales, reflected in predicted changes in behavioral outputs that depend on the specific developmental window. It has previously been shown that during development, *C. elegans* individuals exhibit temporal patterns of long-term behavior that are highly dynamic across and within developmental stages, shaped by both the neuromodulatory state of the population and its environmental experiences (Stern et al., 2017; Harel et al., 2024; Ali Nasser et al., 2023). In this work, by monitoring the temporal synchronization of behavior among multiple isolated *C. elegans* individuals throughout their complete developmental trajectory, we studied how time-locked patterns of behavior are established across distinct developmental stages. In addition, we explored the neuronal alterations within the nervous system that may lead to the impairment of this robust time synchronization. Our results revealed that wild-type individuals showed variable levels of temporal synchronization across distinct developmental stages. Interestingly, while individuals exhibited near-random temporal patterns of roaming over time during the first larval stage, synchronization of behavioral patterns gradually increased during later larval stages. These results suggest the developmental consolidation of robust temporal patterns of behavior that are predicted in time. As the *C. elegans* nervous system is being shaped during post-embryonic development, both at the cell state (Ripoll-Sánchez et al., 2023; Sun and Hobert, 2021; Taylor et al., 2021) and structural level (Sulston and Horvitz, 1977; White et al., 1986; Witvliet et al., 2021) to affect behavior, the increase in the robustness of time-locked behavioral patterns across developmental stages may reflect the control of temporally-synchronized behaviors by the function of specific circuits.

Following this hypothesis, we sought to identify neuronal processes that may impair the temporal structure of behavior and its consolidation across developmental

stages. By testing the temporal synchronization levels in mutant populations, where the function or structure of the nervous system is perturbed, we found multiple instances of impaired behavioral synchronization. For example, mutants for the epigenetic chromatin modifiers *hpl-1* and *met-2* that are known to be expressed within the *C. elegans* nervous system (Taylor et al., 2021) showed lower time synchronization compared to the wild-type, indicating their relatively unstructured behavior over time. Epigenetic mechanisms were shown to act within neurons to control developmental timing of cell maturation (Ciceri et al., 2024). It is plausible that epigenetic alterations within neuronal circuits destabilize cellular states required for establishing developmentally synchronized behavioral patterns. In contrast, we also found cases in which long-term behavioral patterns across individuals became more time-synchronized within specific mutant populations. For instance, mutants for *osm-9* or *tax-4* that are known to be involved in multiple sensory modalities (Bargmann et al., 1993; Colbert et al., 1997; Dusenbery et al., 1975; Mori and Ohshima, 1995) showed higher temporal correlations, across most of the developmental stages or during specific stages, respectively. The increase in temporal synchronization in these sensory mutants implies that environmental inputs may also play a role in tuning behavioral time-synchronization. These results suggest that multiple neuronal perturbations can modify the levels of robustness of developmental structures of behavior, further emphasizing the control of time-locked behavioral patterns across development by the *C. elegans* nervous system.

In addition to gene mutants that affect neuronal states, we also tested neurodegenerative mutants in which hyperactive forms of *mec-4*, *deg-1* and *deg-3* lead to neurodegeneration of specific circuits relatively early in development (Chalfie and Wolinsky, 1990; Driscoll and Chalfie, 1991; Treinin and Chalfie, 1995). We found that all three mutants, despite acting via variable mechanisms for generating neurodegeneration, showed strong impairment of the temporal structure of behavior. By following up on one of the cases in which a hyperactive form of *mec-4* leads to neurodegeneration of six touch receptors neurons (TRN) we further found that either pharmacological or genetic neuroprotection from degeneration reestablished normal developmental structures of behavior. These results imply that even within the relatively compact nervous system of *C. elegans*, the degeneration of local neuronal circuits

alters the normal developmental patterns of behavior. Neurodegenerative processes have been linked to multiple slow-progressing diseases in humans (Wilson et al., 2023). Similarly, the relatively long timescales of the underlying cellular neurodegenerative process in *C. elegans* may lead to impaired long-term behavior that spans multiple life stages.

To further ask what are the effects of the local TRN degeneration on the underlying neuronal activity patterns of other circuits within the nervous system, we analyzed the spontaneous activity patterns of tens of downstream ventral nerve cord (VNC) motor neurons in the neurodegenerative mutants, as well as in wild-type individuals where the TRN circuit is intact. We found alterations in the activity patterns of the VNC motor neurons in individuals in which the TRN circuit is degenerated, including the increase in their activity amplitudes and the longer duration of neuronal activity bouts. The VNC motor neurons are directly involved in executing motor programs with most being defined during post-embryonic development. It is plausible that an early local degeneration process in the TRN circuit may lead to the modifications of multiple circuits within the network, including the VNC motor neurons.

More broadly, these results suggest that while under the normal context of an intact nervous system, individuals show highly similar temporal behavioral patterns, functional or structural perturbations within the nervous system may generate temporal diversity in behavior. We hypothesize that on evolutionary timescales, this exposed temporal behavioral diversity within populations may serve as phenotypic parameter that may drive modifications in the nervous system towards alternative patterns of long-term behaviors.

Methods

C. elegans populations

C. elegans strains used in this study: Wild-type Bristol N2; ZB1028 *crt-1(bz29)* V; TU1948 *deg-1(u38)* X; TU1747 *deg-3(u662)* V; *SST246 mec-4(u231)* X*; crt-1(bz29)* V (*mec-4*::GFP crossed out from ZB1602); CB1611 *mec-4(1611)* X; CB1339 *mec-4(e1339)* X; TU231 *mec-4(u231)* X; TU253 *mec-4(u253)* X; MT15434 *tph-1(mg280)* II; MT1522 *ced-3(n717)* IV; KP4 *glr-1(n2461)* III; MT13971 *hpl-1(n4317)* X*;* MT13293 *met-2(n4256)* III; DA609 *npr-1(ad609)* X*;* CX10 *osm-9(ky10)* IV; PR678 *tax4*(p678) III; MT10661 *tdc-1(n3420)* II; CB1112 *cat-2(e1112)* II; HisCl strain: SST243 *stsEx*044 [*mec-4p::HisCl1::SL2:GFP* (50 ng/µl)*; Pmyo-2::mCherry::unc-54utr* (5 ng/µl)]. Neuronal imaging strains: OH16230 *otIs670[NeuroPAL], otIs672[panneuronal::GCaMP6s];* SST116 *mec-4(u231); otIs670[NeuroPAL]; otIs672[panneuronal::GCaMP6s]* was generated by crossing TU231 strain with OH16230 strain.

Plasmids

pLL013 (*mec-4p::HisCl1::SL2:GFP*) was generated by replacing the promoter in *pNP472* (Pokala et al., 2014) with 1069 bp of *mec-4* promoter amplified from *Pmec-4::lin-14* plasmid (Ritchie et al., 2017).

Growth conditions

C. elegans worms were maintained on NGM agar plates, supplemented with E. coli OP50 bacteria as a food source. For behavioral tracking, we imaged single individuals grown from egg-hatching to adulthood in custom-made laser-cut multi-well plates. Each well (10mm in diameter) was seeded with a specified amount of OP50 bacteria (10 µL of 1.5 OD) that was UV-killed before the experiment to prevent bacterial growth during the experiment. For the amiloride supplementation experiments, 30µL of amiloride (10mM) (Sigma, A7410) was applied to each well in the imaging plates after bacterial seeding and UV illumination. In addition, the source plates used for embryos extraction contained OP50 with a concentration of 10mM amiloride. For the HisCl chemogenetic

experiments (Pokala et al., 2014), 10µl of Histamine (200mM) (Sigma, H7250) was applied to each well in the imaging plates after bacterial seeding and UV illumination.

Behavioral imaging system

Longitudinal behavioral imaging was performed using custom-made imaging systems. Each imaging system consists of an array of six 12 MP USB3 cameras (FLIR, Flea3) and 35 mm high-resolution objectives (Edmund optics) mounted on optical construction rails (Thorlabs). Each camera images six individual wells. Movies are captured at 3 fps with a spatial resolution of ~9.5 um. For homogenous illumination of the imaging plates we used identical LED backlights (Metaphase Technologies) and polarization sheets. Imaging was conducted inside a custom-made environmental chamber in which temperature was controlled using a Peltier element (TE technologies, temperature fluctuations in the range of 22.5 ± 0.1°C). Humidity was held in the range of 50% +/− 5% with a sterile water reservoir and outside illumination was blocked, keeping the internal LED backlights as the only illumination source. Movies from the cameras were captured using commercial software (FlyCapture, FLIR) and saved on two computers (3 cameras per computer).

Extraction of developmental trajectories of behavior

To extract behavioral trajectories of each individual's center of mass across the experiment, captured videos were analyzed by a custom-made script programmed in MATLAB (Mathworks) (Stern et al. 2017). In each video frame, each individual worm is automatically detected as a moving object in space by background subtraction, and the coordinates of its visual center of mass are logged. In each experiment, 600,000-700,000 frames per individual are analyzed using ~50 processor cores to reconstruct the full behavioral trajectory over days of measurements across all stages of development. The total time of image processing was 3-4 days for tens of individuals per experiment across the full developmental trajectory. Egg hatching time of each individual is automatically marked by the time when activity can be detected in the arena. The middle of the lethargus periods were manually identified as the transition points between different stages of development (based on 10s-time-scale speed

trajectories, smoothed over 300 frames). To align the temporal behavioral trajectories of different individuals we age-normalized individuals by dividing the behavioral trajectory of each developmental stage into a fixed number of time windows.

Quantification of behavioral parameters

For each individual, we differentiate between roaming and dwelling locomotory states by averaging speed (μm/s) and angular velocity (absolute deg/s) over 10 seconds using a moving time window, and generating a 2D probability distribution of these two behavioral parameters for all intervals in each time-bin along the experiment (50 X 50 bins distribution, speed bin size: 7.59 um/s, angular velocity bin size: 3.6 deg/s) (Stern et al., 2017). Drawing a diagonal through the probability distribution separated roaming and dwelling states (Arous et al., 2009; Flavell et al., 2013; Stern et al., 2017). The behavior of each animal across time was quantified as a sequence of roaming and dwelling intervals. The fraction of time spent roaming represents the fraction of these intervals classified as roaming states within a given time bin. For each developmental stage, we quantified the two-dimensional probability distribution of the whole population and changed the slope of the diagonal to classify roaming and dwelling appropriately (slopes: 5,2.5,2.3,2,1.5 for the L1,L2,L3,L4 and adult stages, respectively). To analyze the temporal synchronization in roaming behavior we quantified the Pearson correlation among each pair of individuals (pairwise temporal correlations) within the population. For comparing the temporal correlations between populations and across developmental stages, the average temporal correlation between each individual and all other individuals in the population was quantified.

Microscopy and neuronal imaging

For neuronal GCaMP imaging, individual NeuroPAL worms (Yemini et al., 2021) were transferred to a non-seeded NGM plate for 5 minutes to remove residual bacteria, then mounted on a slide with a 2% agar pad and immobilized using 5 mM tetramisole in M9 buffer.

Ventral nerve cord motor neurons were imaged using a Nikon Eclipse Ti2 inverted microscope and 40X objective (NA 0.95). Initial images for neuronal positioning in

individuals were captured for pan-neuronal RFP fluorescence. For L4 individuals, imaging neuronal activity was performed by tracking GCaMP fluorescence at 1 Hz for 10 minutes. For L2 individuals, imaging neuronal activity was performed at 0.5 Hz for 15 minutes. Images were taken following the RVG site to the posterior end. The number of VNC motor neurons that were captured in each individual varied due to worm's position on the slide.

Neuronal activity analysis was performed using Fiji software. Neuronal positions were manually marked using the acquired pan-neuronal RFP images. $\Delta F/F_0$ was calculated for each neuron (F_0 defined as the 10th percentile) and data were smoothed using a moving median (10 bins). Neuronal activity thresholds were determined using the Otsu method via MATLAB's 'multithresh' function as previously described (Ji et al., 2021). Identification of VNC neurons was performed manually in L4 individuals based on the neuronal position map (Skuhersky et al., 2022). Identification of single neurons was not performed in L2 individuals due to larger positional variation. Activity bouts were defined as contiguous periods where $\Delta F/F_0$ values remained above the threshold, bounded by values below the threshold. Based on the identified activity bouts across neurons, averages of activity intensity during bouts ($\Delta F/F_0$), bouts duration, and bouts frequency were quantified

Acknowledgments

We thank Monica Driscoll, Cori Bargmann, and Massimo Hilliard for sharing strains and plasmids. We thank members of our laboratory for discussions and comments on the manuscript. Some strains were provided by the CGC, which is funded by the NIH Office of Research Infrastructure Programs (P40 OD010440). This work was supported by the European Research Council ERC-2019-STG and the Israel Science Foundation grant 3035/20.

References

Ali Nasser, R., Harel, Y., Stern, S., 2023. Early-life experience reorganizes neuromodulatory regulation of stage-specific behavioral responses and individuality dimensions during development. eLife 12, e84312. https://doi.org/10.7554/eLife.84312

Andersen, E.C., Horvitz, H.R., 2007. Two *C. elegans* histone methyltransferases repress *lin-3* EGF transcription to inhibit vulval development. Development 134, 2991–2999. https://doi.org/10.1242/dev.009373

Arous, J.B., Laffont, S., Chatenay, D., 2009. Molecular and Sensory Basis of a Food Related Two-State Behavior in C. elegans. PLOS ONE 4, e7584. https://doi.org/10.1371/journal.pone.0007584

Bargmann, C.I., Hartwieg, E., Horvitz, H.R., 1993. Odorant-selective genes and neurons mediate olfaction in C. elegans. Cell 74, 515–527. https://doi.org/10.1016/0092-8674(93)80053-H

Ben Arous, J., Laffont, S., Chatenay, D., 2009. Molecular and sensory basis of a food related two-state behavior in C. elegans. PloS One 4, e7584. https://doi.org/10.1371/journal.pone.0007584

Bianchi, L., Gerstbrein, B., Frøkjær-Jensen, C., Royal, D.C., Mukherjee, G., Royal, M.A., Xue, J., Schafer, W.R., Driscoll, M., 2004. The neurotoxic MEC-4(d) DEG/ENaC sodium channel conducts calcium: implications for necrosis initiation. Nat. Neurosci. 7, 1337–1344. https://doi.org/10.1038/nn1347

Brown, A.L., Fernandez-Illescas, S.M., Liao, Z., Goodman, M.B., 2007. Gain-of-function mutations in the MEC-4 DEG/ENaC sensory mechanotransduction channel alter gating and drug blockade. J. Gen. Physiol. 129, 161–173. https://doi.org/10.1085/jgp.200609672

Chalfie, M., Sulston, J., 1981. Developmental genetics of the mechanosensory neurons of Caenorhabditis elegans. Dev. Biol. 82, 358–370. https://doi.org/10.1016/0012-1606(81)90459-0

Chalfie, M., Wolinsky, E., 1990. The identification and suppression of inherited neurodegeneration in Caenorhabditis elegans 345.

Ciceri, G., Baggiolini, A., Cho, H.S., Kshirsagar, M., Benito-Kwiecinski, S., Walsh, R.M., Aromolaran, K.A., Gonzalez-Hernandez, A.J., Munguba, H., Koo, S.Y., Xu, N., Sevilla, K.J., Goldstein, P.A., Levitz, J., Leslie, C.S., Koche, R.P., Studer, L., 2024. An epigenetic barrier sets the timing of human neuronal maturation. Nature 626, 881–890. https://doi.org/10.1038/s41586-023-06984-8

Colbert, H.A., Smith, T.L., Bargmann, C.I., 1997. OSM-9, a novel protein with structural similarity to channels, is required for olfaction, mechanosensation, and olfactory adaptation in Caenorhabditis elegans. J. Neurosci. Off. J. Soc. Neurosci. 17, 8259–8269. https://doi.org/10.1523/JNEUROSCI.17-21-08259.1997

Couteau, F., Guerry, F., Müller, F., Palladino, F., 2002. A heterochromatin protein 1 homologue in *Caenorhabditis elegans* acts in germline and vulval development. EMBO Rep. 3, 235–241. https://doi.org/10.1093/embo-reports/kvf051

Cueva, J.G., Mulholland, A., Goodman, M.B., 2007. Nanoscale organization of the MEC-4 DEG/ENaC sensory mechanotransduction channel in Caenorhabditis

elegans touch receptor neurons. J. Neurosci. Off. J. Soc. Neurosci. 27, 14089–14098. https://doi.org/10.1523/JNEUROSCI.4179-07.2007
Daly, M., Behrends, P.R., Wilson, M.I., Jacobs, L.F., 1992. Behavioural modulation of predation risk: moonlight avoidance and crepuscular compensation in a nocturnal desert rodent, Dipodomys merriami. Anim. Behav. 44, 1–9. https://doi.org/10.1016/S0003-3472(05)80748-1
Driscoll, M., Chalfie, M., 1991. The mec-4 gene is a member of a family of Caenorhabditi, eiegans genes that can mutate to induce neuronal degeneration 349.
Dusenbery, D.B., Sheridan, R.E., Russell, R.L., 1975. CHEMOTAXIS-DEFECTIVE MUTANTS OF THE NEMATODE *CAENORHABDITIS ELEGANS*. Genetics 80, 297–309. https://doi.org/10.1093/genetics/80.2.297
Ellis, H.M., Horvitz, H.R., 1986. Genetic control of programmed cell death in the nematode C. elegans. Cell 44, 817–829. https://doi.org/10.1016/0092-8674(86)90004-8
Flavell, S.W., Pokala, N., Macosko, E.Z., Albrecht, D.R., Larsch, J., Bargmann, C.I., 2013. Serotonin and the Neuropeptide PDF Initiate and Extend Opposing Behavioral States in C. elegans. Cell 154, 1023–1035. https://doi.org/10.1016/j.cell.2013.08.001
Fujiwara, M., Sengupta, P., McIntire, S.L., 2002. Regulation of body size and behavioral state of C. elegans by sensory perception and the EGL-4 cGMP-dependent protein kinase. Neuron 36, 1091–1102. https://doi.org/10.1016/s0896-6273(02)01093-0
Geffeney, S.L., Cueva, J.G., Glauser, D.A., Doll, J.C., Lee, T.H.-C., Montoya, M., Karania, S., Garakani, A.M., Pruitt, B.L., Goodman, M.B., 2011. DEG/ENaC but Not TRP Channels Are the Major Mechanoelectrical Transduction Channels in a C. elegans Nociceptor. Neuron 71, 845–857. https://doi.org/10.1016/j.neuron.2011.06.038
Goodman, M.B., Ernstrom, G.G., Chelur, D.S., O'Hagan, R., Yao, C.A., Chalfie, M., 2002. MEC-2 regulates C. elegans DEG/ENaC channels needed for mechanosensation. Nature 415, 1039–1042. https://doi.org/10.1038/4151039a
Gwinner, E., 1986. Circannual Rhythms in the Control of Avian Migrations, in: Advances in the Study of Behavior. Elsevier, pp. 191–228. https://doi.org/10.1016/S0065-3454(08)60191-6
Hall, D.H., Gu, G., García-Añoveros, J., Gong, L., Chalfie, M., Driscoll, M., 1997. Neuropathology of Degenerative Cell Death in *Caenorhabditis elegans*. J. Neurosci. 17, 1033–1045. https://doi.org/10.1523/JNEUROSCI.17-03-01033.1997
Harel, Y., Nasser, R.A., Stern, S., 2024. Mapping the developmental structure of stereotyped and individual-unique behavioral spaces in C. elegans. Cell Rep. 43, 114683. https://doi.org/10.1016/j.celrep.2024.114683
Ji, N., Madan, G.K., Fabre, G.I., Dayan, A., Baker, C.M., Kramer, T.S., Nwabudike, I., Flavell, S.W., 2021. A neural circuit for flexible control of persistent behavioral states. eLife 10, e62889. https://doi.org/10.7554/eLife.62889
Kato, S., Kaplan, H.S., Schrödel, T., Skora, S., Lindsay, T.H., Yemini, E., Lockery, S., Zimmer, M., 2015. Global brain dynamics embed the motor command sequence

of Caenorhabditis elegans. Cell 163, 656–669. https://doi.org/10.1016/j.cell.2015.09.034
Kimmel, C.B., Patterson, J., Kimmel, R.O., 1974. The development and behavioral characteristics of the startle response in the zebra fish. Dev. Psychobiol. 7, 47–60. https://doi.org/10.1002/dev.420070109
Kondo, N., Sekijima, T., Kondo, J., Takamatsu, N., Tohya, K., Ohtsu, T., 2006. Circannual Control of Hibernation by HP Complex in the Brain. Cell 125, 161–172. https://doi.org/10.1016/j.cell.2006.03.017
Konopka, R.J., Benzer, S., 1971. Clock Mutants of *Drosophila melanogaster*. Proc. Natl. Acad. Sci. 68, 2112–2116. https://doi.org/10.1073/pnas.68.9.2112
Mori, I., Ohshima, Y., 1995. Neural regulation of thermotaxis in Caenorhabditis elegans. Nature 376, 344–348. https://doi.org/10.1038/376344a0
Morrison, D.W., 1978. Lunar phobia in a neotropical fruit bat, Artibevs jamaicensis (Chiroptera: Phyllostomidae). Anim. Behav. 26, 852–855. https://doi.org/10.1016/0003-3472(78)90151-3
Mulcahy, B., Witvliet, D.K., Mitchell, J., Schalek, R., Berger, D.R., Wu, Y., Holmyard, D., Lu, Y., Ahamed, T., Samuel, A.D.T., Chisholm, A.D., Lichtman, J.W., Zhen, M., 2022. Post-embryonic remodeling of the C. elegans motor circuit. Curr. Biol. CB 32, 4645-4659.e3. https://doi.org/10.1016/j.cub.2022.09.065
O'Hagan, R., Chalfie, M., Goodman, M.B., 2005. The MEC-4 DEG/ENaC channel of Caenorhabditis elegans touch receptor neurons transduces mechanical signals. Nat. Neurosci. 8, 43–50. https://doi.org/10.1038/nn1362
Panda, S., Antoch, M.P., Miller, B.H., Su, A.I., Schook, A.B., Straume, M., Schultz, P.G., Kay, S.A., Takahashi, J.S., Hogenesch, J.B., 2002. Coordinated Transcription of Key Pathways in the Mouse by the Circadian Clock. Cell 109, 307–320. https://doi.org/10.1016/S0092-8674(02)00722-5
Park, B.-J., Lee, D.-G., Yu, J.-R., Jung, S., Choi, K., Lee, Jungsoo, Lee, Jiyeon, Kim, Y.S., Lee, J.I., Kwon, J.Y., Lee, Junho, Singson, A., Song, W.K., Eom, S.H., Park, C.-S., Kim, D.H., Bandyopadhyay, J., Ahnn, J., 2001. Calreticulin, a Calcium-binding Molecular Chaperone, Is Required for Stress Response and Fertility in *Caenorhabditis elegans*. Mol. Biol. Cell 12, 2835–2845. https://doi.org/10.1091/mbc.12.9.2835
Pattwell, S.S., Duhoux, S., Hartley, C.A., Johnson, D.C., Jing, D., Elliott, M.D., Ruberry, E.J., Powers, A., Mehta, N., Yang, R.R., Soliman, F., Glatt, C.E., Casey, B.J., Ninan, I., Lee, F.S., 2012. Altered fear learning across development in both mouse and human. Proc. Natl. Acad. Sci. 109, 16318–16323. https://doi.org/10.1073/pnas.1206834109
Pokala, N., Liu, Q., Gordus, A., Bargmann, C.I., 2014. Inducible and titratable silencing of Caenorhabditis elegans neurons in vivo with histamine-gated chloride channels. Proc. Natl. Acad. Sci. U. S. A. 111, 2770–2775. https://doi.org/10.1073/pnas.1400615111
Ripoll-Sánchez, L., Watteyne, J., Sun, H., Fernandez, R., Taylor, S.R., Weinreb, A., Bentley, B.L., Hammarlund, M., Miller, D.M., Hobert, O., Beets, I., Vértes, P.E., Schafer, W.R., 2023. The neuropeptidergic connectome of C. elegans. Neuron 111, 3570-3589.e5. https://doi.org/10.1016/j.neuron.2023.09.043

Ritchie, F.K., Knable, R., Chaplin, J., Gursanscky, R., Gallegos, M., Neumann, B., Hilliard, M.A., 2017. The Heterochronic Gene lin-14 Controls Axonal Degeneration in C. elegans Neurons. Cell Rep. 20, 2955–2965. https://doi.org/10.1016/j.celrep.2017.08.083

Skuhersky, M., Wu, T., Yemini, E., Nejatbakhsh, A., Boyden, E., Tegmark, M., 2022. Toward a more accurate 3D atlas of C. elegans neurons. BMC Bioinformatics 23, 195. https://doi.org/10.1186/s12859-022-04738-3

Sokolowski, M.B., Kent, C., Wong, J., 1984. Drosophila larval foraging behaviour: Developmental stages. Anim. Behav. 32, 645–651. https://doi.org/10.1016/S0003-3472(84)80139-6

Stern, S., Kirst, C., Bargmann, C.I., 2017b. Neuromodulatory Control of Long-Term Behavioral Patterns and Individuality across Development. Cell 171, 1649-1662.e10. https://doi.org/10.1016/j.cell.2017.10.041

Sulston, J.E., Horvitz, H.R., 1977. Post-embryonic cell lineages of the nematode, Caenorhabditis elegans. Dev. Biol. 56, 110–156. https://doi.org/10.1016/0012-1606(77)90158-0

Sun, H., Hobert, O., 2021. Temporal transitions in the post-mitotic nervous system of Caenorhabditis elegans. Nature 600, 93–99. https://doi.org/10.1038/s41586-021-04071-4

Suzuki, H., Kerr, R., Bianchi, L., Frøkjær-Jensen, C., Slone, D., Xue, J., Gerstbrein, B., Driscoll, M., Schafer, W.R., 2003. In Vivo Imaging of C. elegans Mechanosensory Neurons Demonstrates a Specific Role for the MEC-4 Channel in the Process of Gentle Touch Sensation. Neuron 39, 1005–1017. https://doi.org/10.1016/j.neuron.2003.08.015

Taylor, S.R., Santpere, G., Weinreb, A., Barrett, A., Reilly, M.B., Xu, C., Varol, E., Oikonomou, P., Glenwinkel, L., McWhirter, R., Poff, A., Basavaraju, M., Rafi, I., Yemini, E., Cook, S.J., Abrams, A., Vidal, B., Cros, C., Tavazoie, S., Sestan, N., Hammarlund, M., Hobert, O., Miller, D.M., 2021. Molecular topography of an entire nervous system. Cell 184, 4329-4347.e23. https://doi.org/10.1016/j.cell.2021.06.023

Treinin, M., Chalfie, M., 1995. A mutated acetylcholine receptor subunit causes neuronal degeneration in C. elegans. Neuron 14, 871–877. https://doi.org/10.1016/0896-6273(95)90231-7

Vance, J.T., Williams, J.B., Elekonich, M.M., Roberts, S.P., 2009. The effects of age and behavioral development on honey bee (*Apis mellifera*) flight performance. J. Exp. Biol. 212, 2604–2611. https://doi.org/10.1242/jeb.028100

Von Stetina, S.E., Treinin, M., Miller, D.M., 2005. The Motor Circuit, in: International Review of Neurobiology. Elsevier, pp. 125–167. https://doi.org/10.1016/S0074-7742(05)69005-8

White, J.G., Southgate, E., Thomson, J.N., Brenner, S., 1986. The structure of the nervous system of the nematode Caenorhabditis elegans. Philos. Trans. R. Soc. Lond. B. Biol. Sci. 314, 1–340. https://doi.org/10.1098/rstb.1986.0056

Wilson, D.M., Cookson, M.R., Van Den Bosch, L., Zetterberg, H., Holtzman, D.M., Dewachter, I., 2023. Hallmarks of neurodegenerative diseases. Cell 186, 693–714. https://doi.org/10.1016/j.cell.2022.12.032

Witvliet, D., Mulcahy, B., Mitchell, J.K., Meirovitch, Y., Berger, D.R., Wu, Y., Liu, Y., Koh, W.X., Parvathala, R., Holmyard, D., Schalek, R.L., Shavit, N., Chisholm, A.D., Lichtman, J.W., Samuel, A.D.T., Zhen, M., 2021. Connectomes across development reveal principles of brain maturation. Nature 596, 257–261. https://doi.org/10.1038/s41586-021-03778-8

Xu, K., Tavernarakis, N., Driscoll, M., 2001. Necrotic Cell Death in C. elegans Requires the Function of Calreticulin and Regulators of Ca2+ Release from the Endoplasmic Reticulum. Neuron 31, 957–971. https://doi.org/10.1016/S0896-6273(01)00432-9

Yemini, E., Lin, A., Nejatbakhsh, A., Varol, E., Sun, R., Mena, G.E., Samuel, A.D.T., Paninski, L., Venkatachalam, V., Hobert, O., 2021. NeuroPAL: A Multicolor Atlas for Whole-Brain Neuronal Identification in C. elegans. Cell 184, 272-288.e11. https://doi.org/10.1016/j.cell.2020.12.012

Figure 1

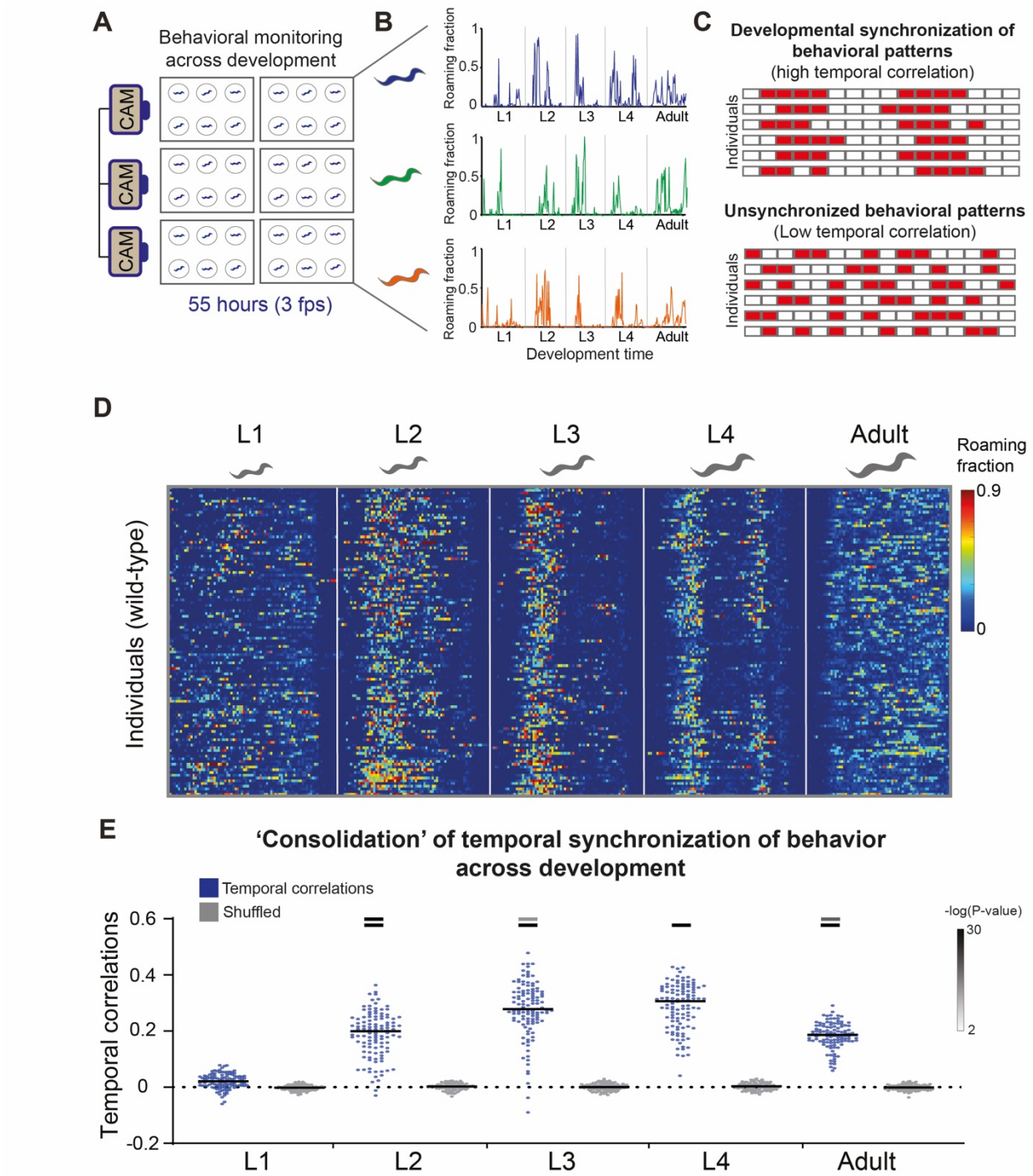
A
Behavioral monitoring across development
CAM
CAM
CAM
55 hours (3 fps)
B
Roaming fraction
1
0.5
0
L1
L2
L3
L4
Adult
Development time
C
Developmental synchronization of behavioral patterns
(high temporal correlation)
Individuals
Unsynchronized behavioral patterns
(Low temporal correlation)
Individuals
D
L1
L2
L3
L4
Adult
Roaming fraction
0.9
0
Individuals (wild-type)
E
'Consolidation' of temporal synchronization of behavior across development
Temporal correlations
Shuffled
-log(P-value)
30
2
Temporal correlations
0.6
0.4
0.2
0
-0.2
L1
L2
L3
L4
Adult

Figure 1. Long-term tracking of *C. elegans* individuals reveals the consolidation of temporal synchronization of behavior across developmental stages

(A) Multi-camera imaging system allows longitudinal behavioral tracking of multiple *C. elegans* individuals throughout a complete development time, at high spatiotemporal resolution and under tightly controlled environmental conditions. **(B)** Shown are representative developmental trajectories of roaming behavior of three individual animals across all four larval stages and adulthood. Age-normalization equally divides each developmental stage into 75 time-bins. **(C)** A scheme representing temporally synchronized (top) and unsynchronized (bottom) behavioral patterns of roaming activity. Each row represents a single individual. Red indicates bouts of active roaming behavior over time. **(D)** Roaming and dwelling behavior of wild-type N2 animals (n=113). Each row indicates the age-normalized behavior of one individual across all developmental stages. Different developmental stages are separated by white lines indicating the middle of the lethargus state. Color bar represents the fraction of time spent roaming in each of the time-bins. **(E)** Temporal correlations of roaming behavior among individuals within the wild-type population (blue) compared to a randomly shuffled dataset (grey) across distinct developmental stages. Each dot represents the average temporal correlation between a single individual and all other individuals in the population. Black bars represent the median correlation. Color bars represent the significance (-log(P-value)) of the difference in temporal correlations between each of the L2-Adult stages to the L1 stage (bottom), and to the previous stage (top) (Wilcoxon rank-sum test, FDR corrected). Indicated are P-values<0.01.

Figure 2

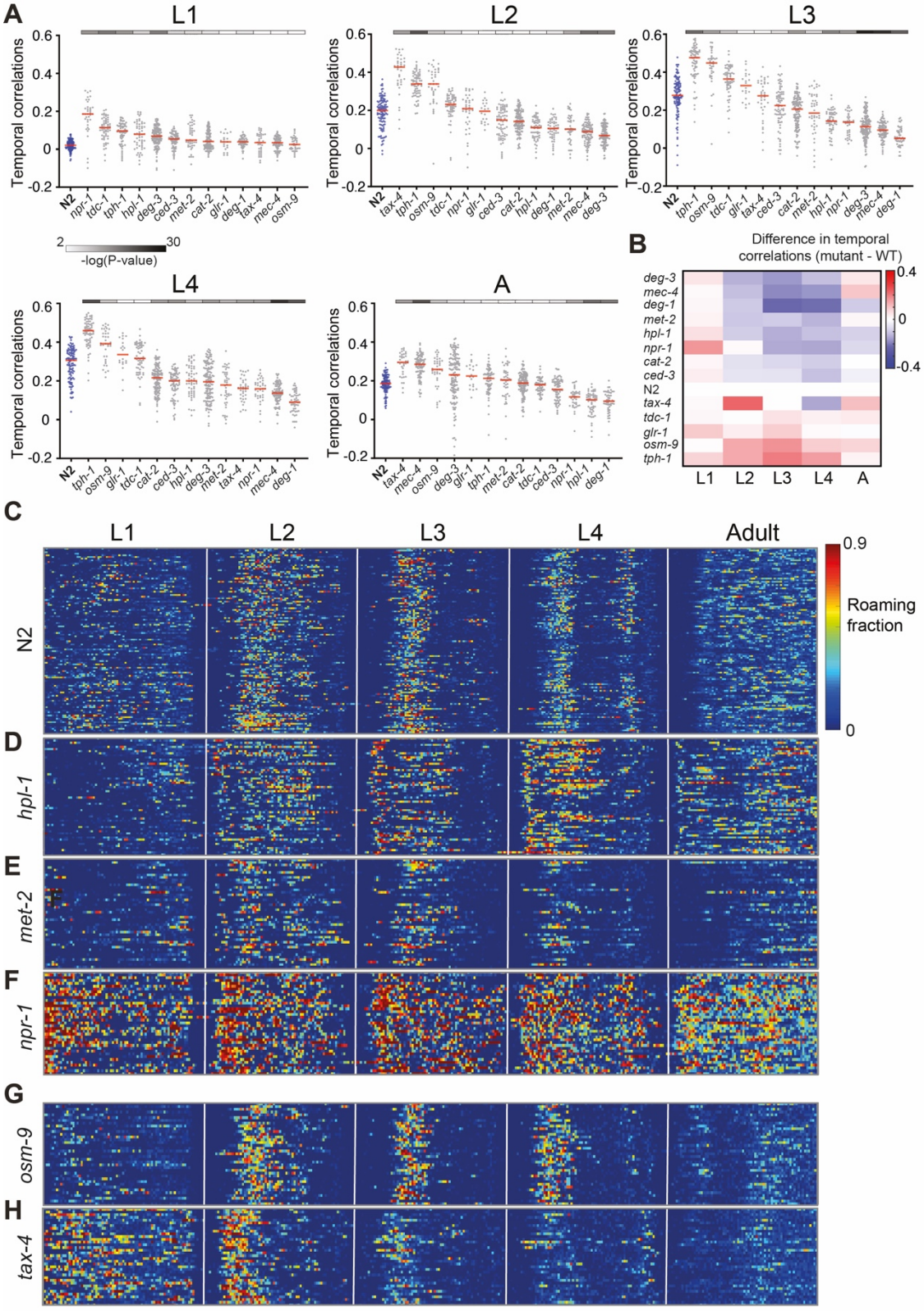
A
L1
L2
L3
L4
A
Temporal correlations
0.6
0.4
0.2
0
-0.2
N2
npr-1
tdc-1
tph-1
hpl-1
deg-3
ced-3
met-2
cat-2
glr-1
deg-1
tax-4
mec-4
osm-9
2
30
-log(P-value)
B
Difference in temporal correlations (mutant - WT)
0.4
0
-0.4
L1
L2
L3
L4
A
C
Adult
0.9
Roaming fraction
0
D
hpl-1
E
met-2
F
npr-1
G
osm-9
H
tax-4

Figure 2. Identification of alterations in behavioral time-synchronization within mutant populations

(A) Temporal correlations of roaming behavior among individuals within the wild-type population (blue) and 13 mutant populations for neuronal genes (grey) in each developmental stage. Each dot represents the average temporal correlation between a single individual and all other individuals in the population. Red bars represent the median correlation across each of the populations. Mutant populations are sorted based on their median temporal correlation for visualization. Color bars (top) represent the significance (-log(P-value)) of the difference in temporal correlations between each of the mutant populations and the wild-type (Wilcoxon rank-sum test, FDR corrected). Indicated are P-values<0.01. **(B)** Difference in median temporal correlation between each of the mutant populations and the wild-type in each developmental stage. **(C-H)** Roaming and dwelling behavior of (C) wild-type, and (D) *hpl-1,* (E) *met-2*, (F) *npr-1*, (G) *osm-9*, (H) *tax-4* mutant individuals. Each row indicates the behavior of one individual across all developmental stages. Different stages are separated by white lines indicating the middle of the lethargus state. Color bar represents the fraction of time spent roaming in each of the time-bins. N2 n=113, *deg-1(u38)* n=51, *mec-4(u231)* n=93, *deg-3(u662)* n=139, *hpl-1(n4317)* n=56, *met-2(n4256)* n=44, *npr-1(ad609)* n=37, *osm-9(ky10)* n=37, *tax-4(p678)* n=36, *ced-3(n717)* n=75, *glr-1(n2461)* n=20, *tph-1(mg280)* n=67, *cat-2(e1112)* n=124, *tdc-1(n3420)* n=60.

Figure 3

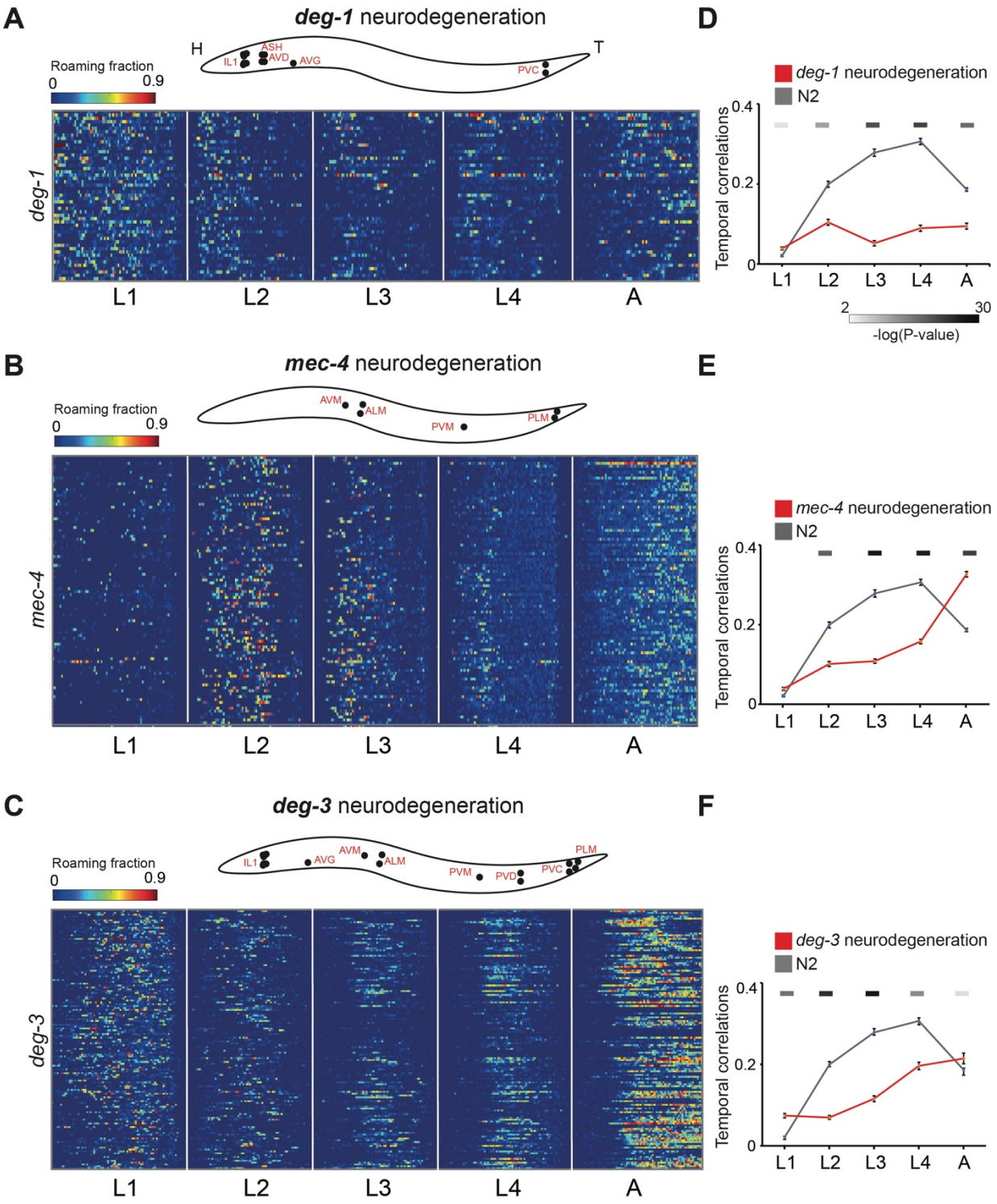
A
deg-1 neurodegeneration
H
T
ASH
IL1
AVD
AVG
PVC
Roaming fraction
0
0.9
deg-1
L1
L2
L3
L4
A
D
deg-1 neurodegeneration
N2
Temporal correlations
0.4
0.2
0
L1
L2
L3
L4
A
2
30
-log(P-value)
B
mec-4 neurodegeneration
AVM
ALM
PVM
PLM
Roaming fraction
0
0.9
mec-4
L1
L2
L3
L4
A
E
mec-4 neurodegeneration
N2
Temporal correlations
0.4
0.2
0
L1
L2
L3
L4
A
C
deg-3 neurodegeneration
IL1
AVG
AVM
ALM
PVM
PVD
PVC
PLM
Roaming fraction
0
0.9
deg-3
L1
L2
L3
L4
A
F
deg-3 neurodegeneration
N2
Temporal correlations
0.4
0.2
0
L1
L2
L3
L4
A

Figure 3. Neurodegeneration impairs the developmental structures of long-term behavior

(A-C) Illustrations of known degenerated neurons (top) and roaming and dwelling behavior (bottom) in (A) *deg-1,* (B) *mec-4*, and (C) *deg-3* neurodegenerative mutant individuals. Each row indicates the behavior of one individual across all developmental stages. Different stages are separated by white lines indicating the middle of the lethargus state. Color bar represents the fraction of time spent roaming in each of the time-bins. 'H' and 'T' mark head and tail, respectively. **(D-F)** Temporal correlations of roaming behavior among individuals within the (D) *deg-1,* (E) *mec-4*, and (F) *deg-3* mutant populations (red), compared to the wild-type (grey), across distinct developmental stages. Error bars represent standard error of the mean. Color bars (top) represent the significance (-log(P-value)) of the difference in temporal correlations between each of the mutant populations and the wild-type (Wilcoxon rank-sum test, FDR corrected). Indicated are P-values<0.01. N2 n=113, *deg-1(u38)* n=51, *mec-4 (u231)* n=93, *deg-3(u662)* n=139.

Figure 4

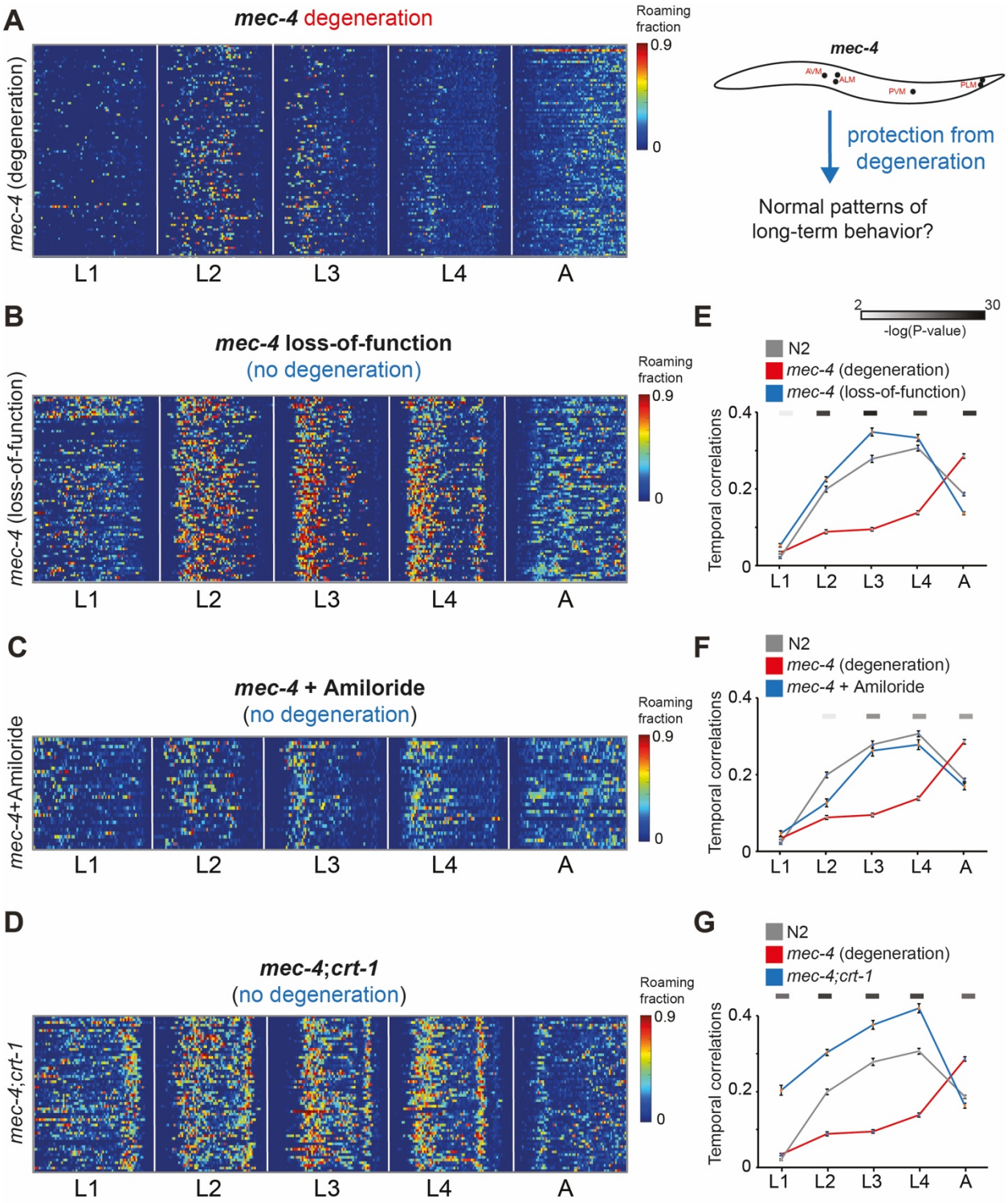
A
mec-4 degeneration
mec-4 (degeneration)
Roaming fraction
0.9
0
L1
L2
L3
L4
A
mec-4
AVM
ALM
PVM
PLM
protection from degeneration
Normal patterns of long-term behavior?
B
mec-4 loss-of-function
(no degeneration)
mec-4 (loss-of-function)
E
2
30
-log(P-value)
N2
mec-4 (degeneration)
mec-4 (loss-of-function)
Temporal correlations
0.4
0.2
0
C
mec-4 + Amiloride
(no degeneration)
mec-4+Amiloride
F
mec-4 + Amiloride
D
mec-4;crt-1
(no degeneration)
mec-4;crt-1
G

Figure 4. Neuroprotection from degeneration reestablishes normal patterns of long-term behavior

(A) Left: Roaming and dwelling behavior in *mec-4* neurodegenerative mutant individuals as in 3B. Each row indicates the behavior of one individual across all developmental stages. Different stages are separated by white lines indicating the middle of the lethargus state. Color bar represents the fraction of time spent roaming in each of the time-bins. Right: Illustration of protection from *mec-4* degeneration. **(B-D)** Roaming and dwelling behavior in (B) *mec-4* loss-of-function mutants *(e1339)* not causing degeneration, (C) *mec-4* neurodegenerative mutants *(u231)* with the supplementation of amiloride, and (D) double mutants for the *mec-4* neurodegenerative mutation *(u231)* and *crt-1(bz29)* mutation. **(E-G)** Temporal correlations of roaming behavior among individuals within the (E) *mec-4* loss-of-function mutants *(e1339)* not causing degeneration, (F) *mec-4* neurodegenerative mutants *(u231)* with the supplementation of amiloride, and (G) double mutants for the *mec-4* neurodegenerative mutation (u231) and *crt-1 (bz29)* mutation (blue), compared to the wild-type (grey) and *mec-4* neurodegenerative mutant individuals *(u231)* (red), across distinct developmental stages. Error bars represent standard error of the mean. Color bars (top) represent the significance (-log(P-value)) of the difference in temporal correlations between each of the neuroprotected populations and the *mec-4* neurodegenerative mutants *(u231)* (Wilcoxon rank-sum test, FDR corrected). Indicated are P-values<0.01.
N2 n=113, *mec-4(u231)* n=93, *mec-4(e1339)* n=93, *mec-4(u231)* + amiloride n=31, *mec-4(u231)*;*crt-1(bz29)* n=58.

Figure 5

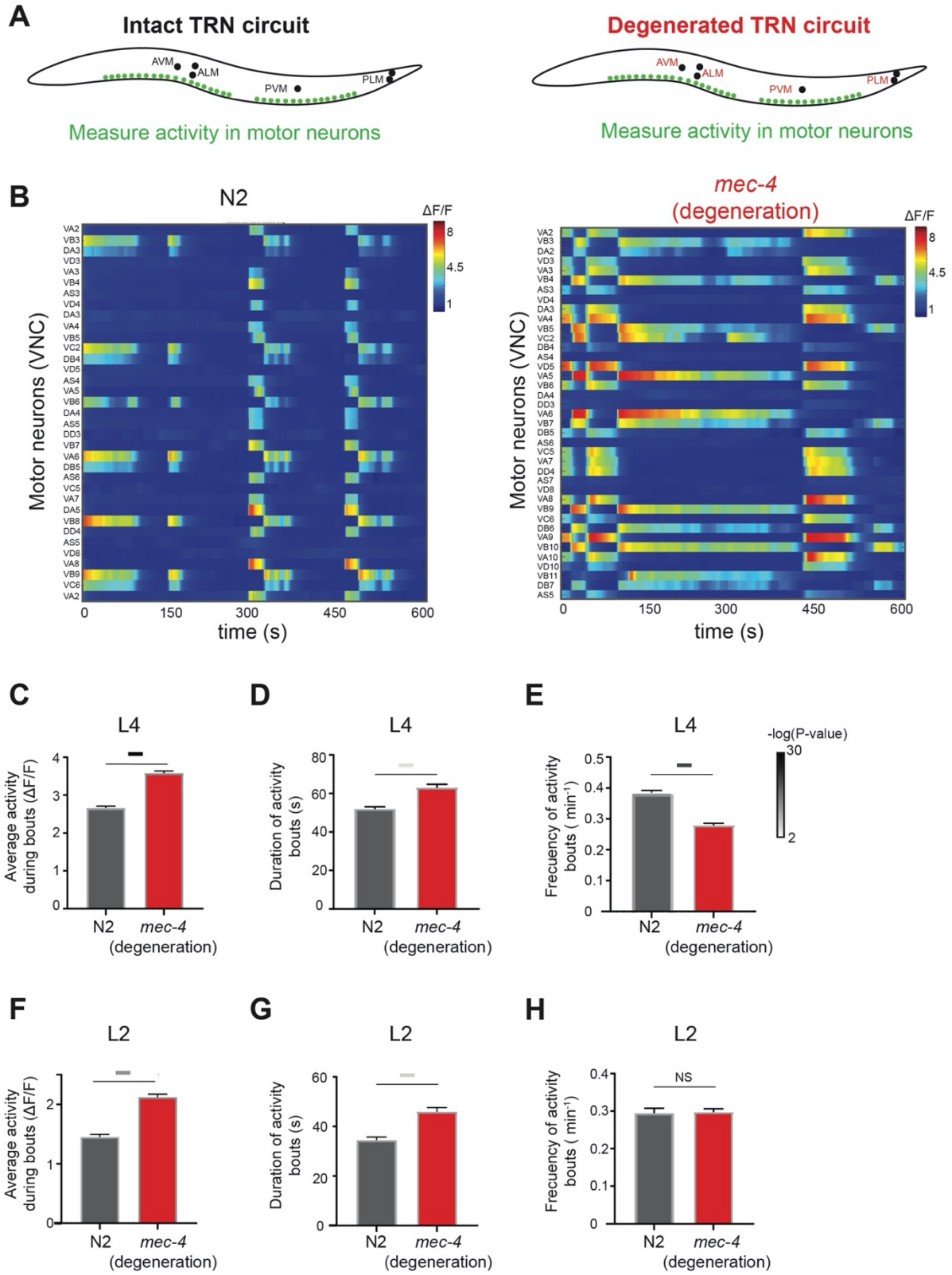
A
Intact TRN circuit
AVM
ALM
PVM
PLM
Measure activity in motor neurons
Degenerated TRN circuit
AVM
ALM
PVM
PLM
Measure activity in motor neurons
B
N2
ΔF/F
8
4.5
1
Motor neurons (VNC)
0
150
300
450
600
time (s)
mec-4
(degeneration)
ΔF/F
8
4.5
1
Motor neurons (VNC)
0
150
300
450
600
time (s)
C
L4
Average activity during bouts (ΔF/F)
N2
mec-4
(degeneration)
D
L4
Duration of activity bouts (s)
N2
mec-4
(degeneration)
E
L4
-log(P-value)
30
2
Frecuency of activity bouts (min-1)
N2
mec-4
(degeneration)
F
L2
Average activity during bouts (ΔF/F)
N2
mec-4
(degeneration)
G
L2
Duration of activity bouts (s)
N2
mec-4
(degeneration)
H
L2
NS
Frecuency of activity bouts (min-1)
N2
mec-4
(degeneration)

Figure 5. Impaired neuronal activity dynamics of motor neurons in TRN neurodegenerative mutants

(A) Scheme representing neuronal activity measurements of VNC motor neurons in N2 wild-type individuals (Left) and *mec-4* neurodegenerative mutants *(u231*) in which the touch receptor neurons are degenerated (Right). **(B)** Heat maps represent examples of spontaneous neuronal activity dynamics in motor neurons of wild-type (Left) and *mec-4* neurodegenerative mutant individuals (Right) across 10 minutes in the L4 stage. Color bar represents neuronal activity ($\Delta F/F$), smoothed using moving median (10 bins). **(C-E)** Average neuronal activity during bouts (C), duration of activity bouts (D), and frequency of activity bouts (E) in motor neurons of L4 *mec-4* neurodegenerative mutants (red), compared to wild-type (grey) (see methods). (**F-H)** Average neuronal activity during bouts (F), duration of activity bouts (G), and frequency of activity bouts (H) in motor neurons of L2 *mec-4* neurodegenerative mutants (red), compared to the wild-type (grey). *mec-4(u231)* neurodegenerative mutants (L4: n=615 neurons, 21 individuals; L2: n=351 neurons 15 individuals). N2 (L4: n=722 neurons, 24 individuals; L2: n=185 neurons, 10 individuals).

Figure S1

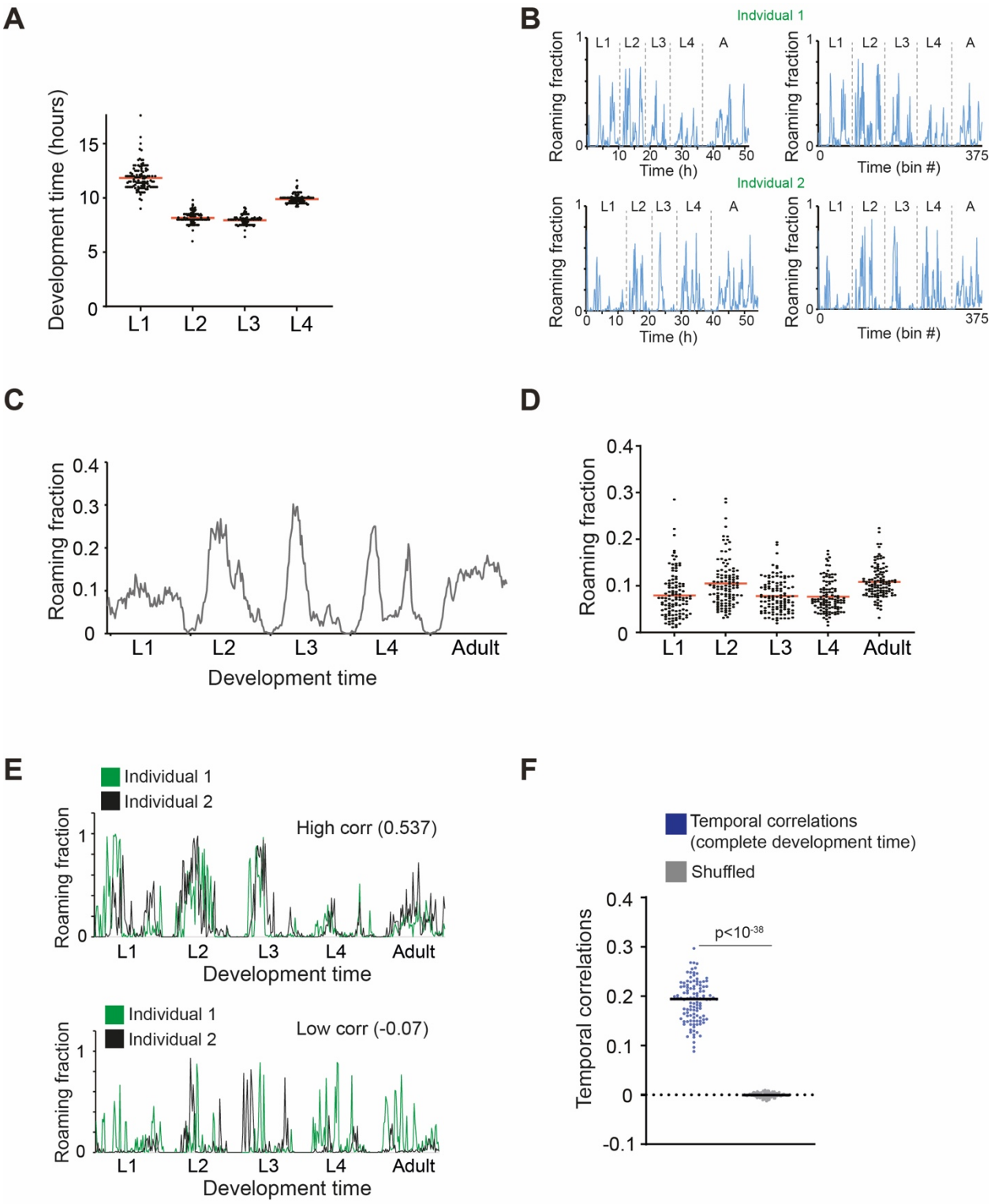
A
Development time (hours)
15
10
5
0
L1
L2
L3
L4
B
Indvidual 1
Roaming fraction
L1
L2
L3
L4
A
Time (h)
Time (bin #)
375
Indvidual 2
C
Roaming fraction
0.4
0.3
0.2
0.1
0
L1
L2
L3
L4
Adult
Development time
D
Roaming fraction
E
Individual 1
Individual 2
High corr (0.537)
Low corr (-0.07)
Development time
F
Temporal correlations
(complete development time)
Shuffled
Temporal correlations
p<10-38
-0.1

Figure S1. Quantification of development-time, average roaming activity and long-term behavioral synchronization across wild-type individuals

(A) Development time across L1-L4 larval stages within the wild-type N2 population (n=113). Each dot represents a single individual. Red bars mark the average across the population. **(B)** Examples of absolute time (left) and age-normalized (right) roaming of two individuals across development. Normalization aligns behavioral trajectories of different individuals across development by dividing each developmental stage of each individual into 75 time-bins. **(C)** Average roaming fraction of wild-type animals across the developmental trajectory (375 time-bins). **(D)** Average roaming fraction of the wild-type population quantified in each developmental stage. Each dot represents a single individual. Red bars mark the average across the population. **(E)** Examples of pairs of wild-type individuals showing relatively high (top) or low (bottom) temporal correlation between their developmental patterns of roaming behavior across a full development time. **(F)** Temporal correlations of roaming behavior among all individuals within the wild-type population (blue) compared to a randomly shuffled dataset (grey), across the complete developmental trajectory. Each dot represents the average temporal correlation between a single individual and all other individuals in the population. Black bar represents the median correlation within the population. P-value calculated by Wilcoxon rank-sum test.

Figure S2

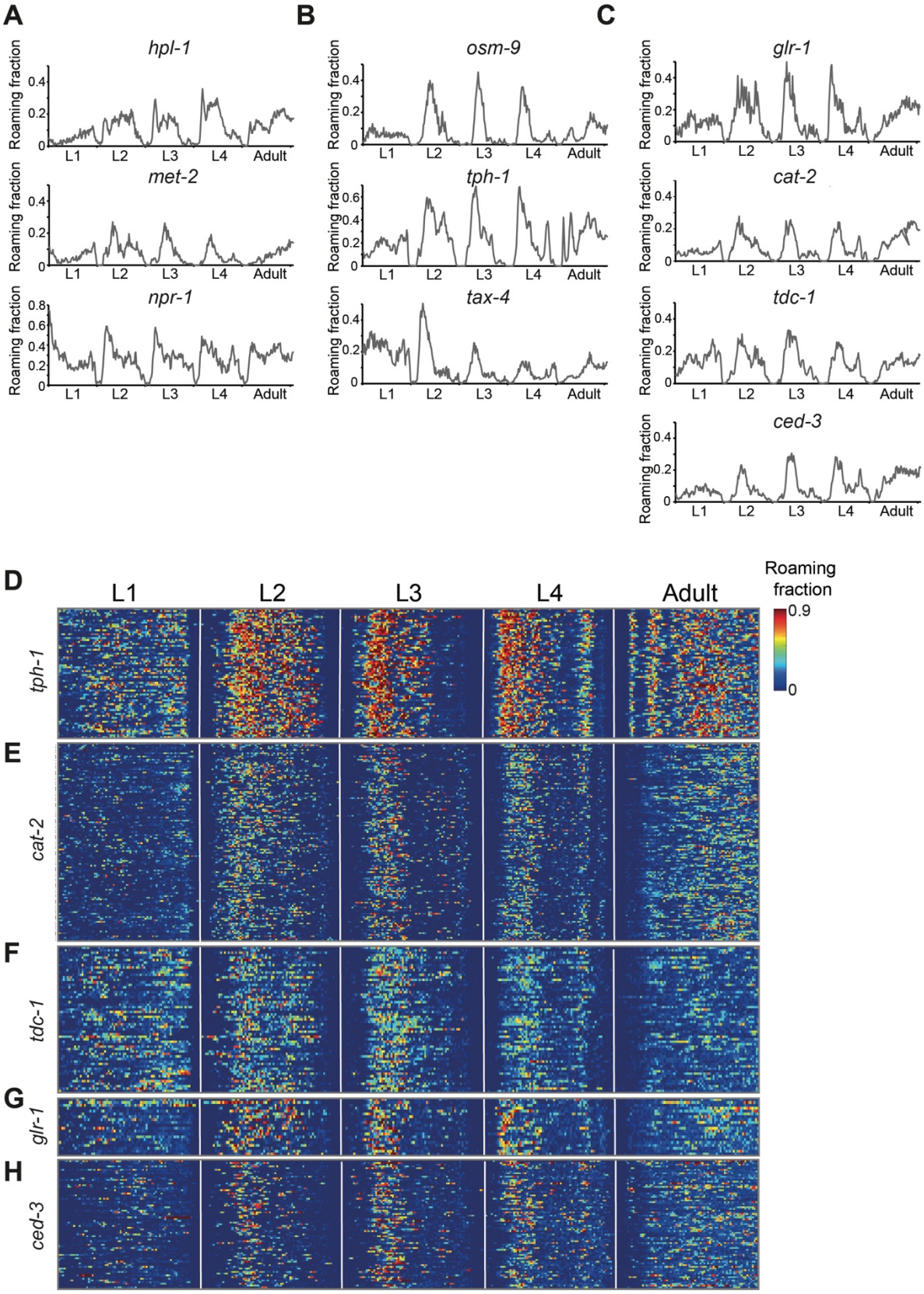
A
B
C
hpl-1
met-2
npr-1
osm-9
tph-1
tax-4
glr-1
cat-2
tdc-1
ced-3
Roaming fraction
L1
L2
L3
L4
Adult
D
E
F
G
H
Roaming fraction
0.9
0

Figure S2. Temporal patterns of roaming activity in neuronal genes mutants

(A-C) Average roaming fraction of (A) *hpl-1*, *met-2, npr-1* (B) *osm-9*, *tph-1*, *tax-4* and (C) *glr-1*, *cat-2*, *tdc-1*, *ced-3* mutant individuals across the developmental trajectory. **(D-H)** Roaming and dwelling behavior in (D) *tph-1*, (E) *cat-2*, (F) *tdc-1*, (G) *glr-1*, and (H) *ced-3* mutant individuals. Each row indicates the behavior of an individual across all developmental stages. Different stages are separated by white lines indicating the middle of the lethargus state. Color bar represents the fraction of time spent roaming in each of the time-bins. *tph-1(mg280)* n=67, *cat-2(e1112)* n=124, *tdc-1(n3420)* n=60; *hpl-1(n4317)* n=56, *met-2(n4256)* n=44, *npr-1(ad609)* n=37, *osm-9(ky10)* n=37, *tax-4(p678)* n=36, *glr-1(n2461)* n=20*; ced-3(n717)* n=75.

Figure S3

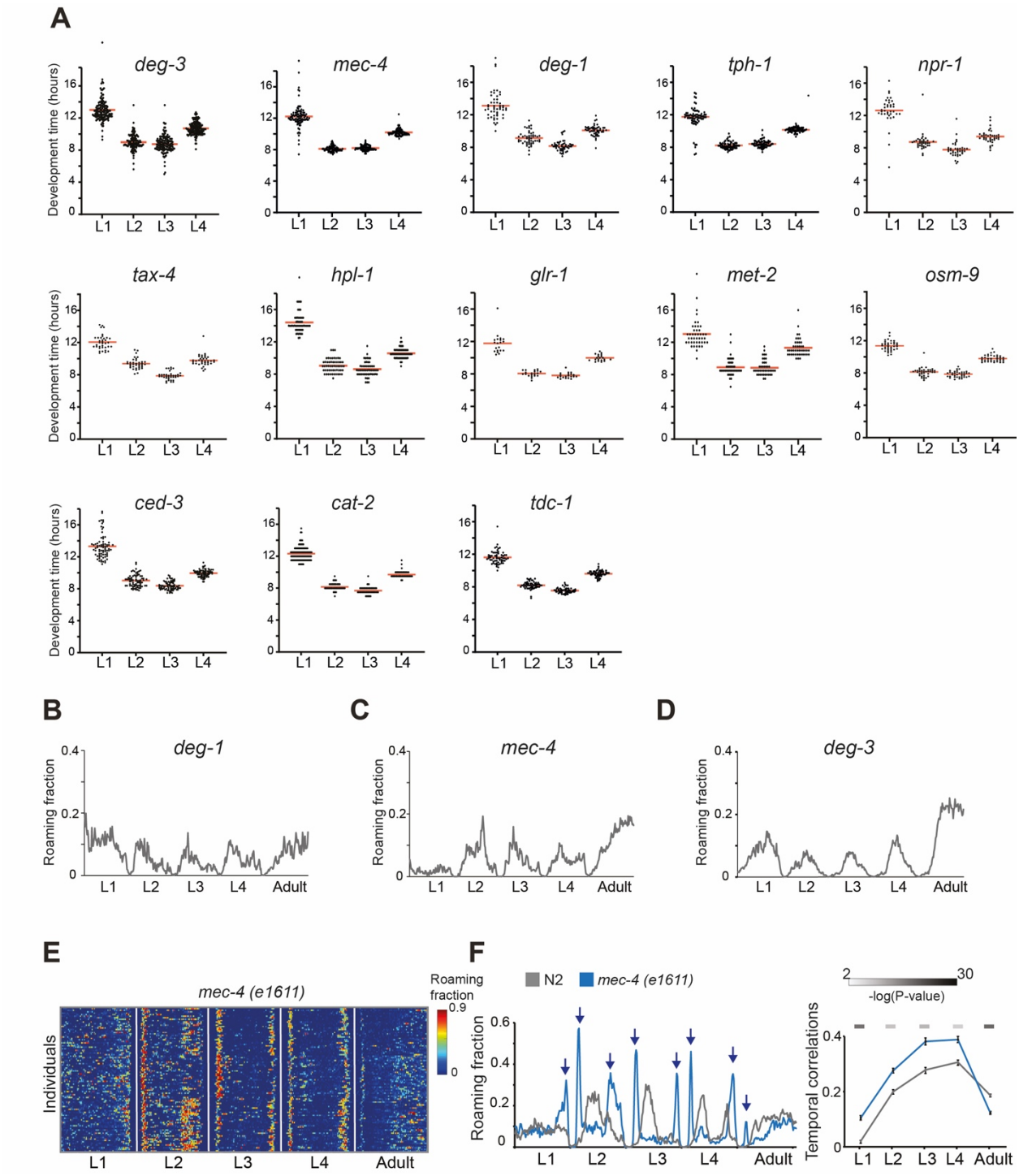
A
deg-3
mec-4
deg-1
tph-1
npr-1
tax-4
hpl-1
glr-1
met-2
osm-9
ced-3
cat-2
tdc-1
Development time (hours)
L1
L2
L3
L4
B
C
D
Roaming fraction
Adult
E
mec-4 (e1611)
Individuals
F
N2
mec-4 (e1611)
Roaming fraction
Temporal correlations
-log(P-value)

Figure S3. Development time in neuronal genes mutants and alterations in long-term patterns of roaming behavior by neurodegeneration

(A) Development time across L1-L4 larval stages within the 13 neuronal genes mutant populations. Each dot represents a single individual. Red bars mark the average across the population. **(B-D)** Average roaming fraction of (B) *deg-1,* (B) *mec-4,* and (C) *deg-3* neurodegenerative mutants across the developmental trajectory. **(E)** Roaming and dwelling behavior in *mec-4(e1611)* individuals. Each row indicates the behavior of one individual across all developmental stages. Different stages are separated by white lines indicating the middle of the lethargus state. Color bar represents the fraction of time spent roaming in each of the time-bins. **(F)** Left**:** Average roaming fraction of *mec-4 (e1611)* individuals across the developmental trajectory. Arrows mark new synchronized peaks of activity in *mec-4(e1611)* mutant individuals (blue), compared to the wild-type population (grey). Right: temporal correlations of roaming behavior in *mec-4(e1611)* individuals, compared to the wild-type population, across distinct developmental stages. Error bars represent standard error of the mean. Color bars (top) represent the significance (-log(P-value)) of the difference in temporal correlations between the mutant population and the wild-type (Wilcoxon rank-sum test, FDR corrected). Indicated are P-values<0.01. N2 n=113, *deg-1(u38)* n=51, *mec-4(u231)* n=93, *deg-3(u662)* n=139, *mec-4(e1611)* n=99, *tph-1(mg280)* n=67, *cat-2(e1112)* n=124, *tdc-1(n3420)* n=60, *hpl-1(n4317)* n=56, *met-2(n4256)* n=44, *npr-1(ad609)* n=37, *osm-9(ky10)* n=37, *tax-4(p678)* n=36, *glr-1(n2461)* n=20*, ced-3(n717)* n=75.

Figure S4

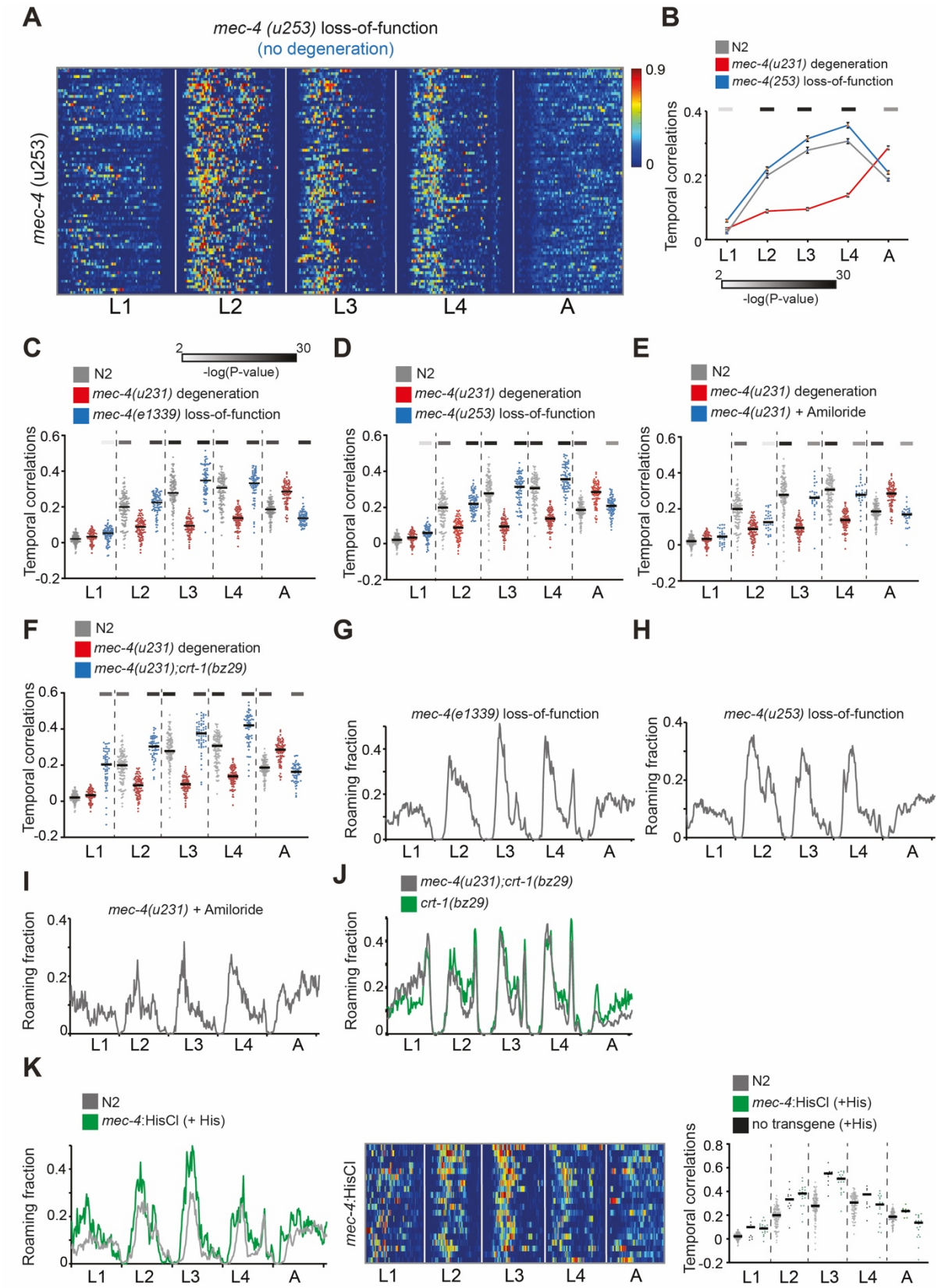
A
mec-4 (u253) loss-of-function
(no degeneration)
mec-4 (u253)
0.9
0
L1
L2
L3
L4
A
B
N2
mec-4(u231) degeneration
mec-4(253) loss-of-function
Temporal correlations
0.4
0.2
0
L1 L2 L3 L4 A
2
30
-log(P-value)
C
2
30
-log(P-value)
N2
mec-4(u231) degeneration
mec-4(e1339) loss-of-function
Temporal correlations
0.6
0.4
0.2
0
-0.2
L1 L2 L3 L4 A
D
N2
mec-4(u231) degeneration
mec-4(u253) loss-of-function
Temporal correlations
L1 L2 L3 L4 A
E
N2
mec-4(u231) degeneration
mec-4(u231) + Amiloride
Temporal correlations
L1 L2 L3 L4 A
F
N2
mec-4(u231) degeneration
mec-4(u231);crt-1(bz29)
Temporal correlations
L1 L2 L3 L4 A
G
mec-4(e1339) loss-of-function
Roaming fraction
0.4
0.2
0
L1 L2 L3 L4 A
H
mec-4(u253) loss-of-function
Roaming fraction
0.4
0.2
0
L1 L2 L3 L4 A
I
mec-4(u231) + Amiloride
Roaming fraction
0.4
0.2
0
L1 L2 L3 L4 A
J
mec-4(u231);crt-1(bz29)
crt-1(bz29)
Roaming fraction
0.4
0.2
0
L1 L2 L3 L4 A
K
N2
mec-4:HisCl (+ His)
Roaming fraction
0.4
0.2
0
L1 L2 L3 L4 A
mec-4:HisCl
L1 L2 L3 L4 A
N2
mec-4:HisCl (+His)
no transgene (+His)
Temporal correlations
0.8
0.6
0.4
0.2
0
-0.2
L1 L2 L3 L4 A

Figure S4. Developmental patterns of behavior following protection from neurodegeneration

(A) Roaming and dwelling behavior in *mec-4* loss-of-function *(u253)* mutant individuals. Each row indicates the behavior of one individual across all developmental stages. Different stages are separated by white lines indicating the middle of the lethargus state. Color bar represents the fraction of time spent roaming in each of the time-bins. **(B)** Temporal correlations of roaming behavior among individuals within the *mec-4* loss-of-function *(u253)* mutants (blue), compared to wild-type (grey) and *mec-4 (u231)* neurodegenerative mutant individuals (red), across distinct developmental stages. Error bars represent standard error of the mean. **(C-F)** Temporal correlations of roaming behavior among individuals within the (C,D) *mec-4* loss-of-function mutants (*e1339* and *u253*), (E) *mec-4* neurodegenerative mutants (*u231*) with the supplementation of amiloride, and (F) double mutants for the *mec-4* neurodegenerative mutation (*u231*) and *crt-1* mutation (*bz29*) (blue), compared to the wild-type (grey) and *mec-4* neurodegenerative mutant (*u231*) individuals (red), across distinct developmental stages. Each dot represents the average temporal correlation between a single individual and all other individuals in the population. Black bars represent the median across each of the populations. **(G-J)** Average roaming fraction of (G,H) *mec-4* loss-of-function mutants (*e1339* and *u253*), (I) *mec-4* neurodegenerative mutants (*u231*) with the supplementation of amiloride, (J) double mutants for the *mec-4* neurodegenerative mutation (*u231*) and *crt-1* mutation (*bz29*) (grey), and single mutants of *crt-1* (*bz29*) (green). **(K)** Left: Average roaming fraction of *mec-4*:HisCl individuals, compared to the wild-type population. Middle: Roaming and dwelling behavior of *mec-4*:HisCl individuals. Right: Temporal correlations of roaming behavior among *mec-4*:HisCl individuals, compared to wild-type individuals and individuals that are exposed to histamine and lack the transgene. Color bars in (B-F) represent the significance (-log(P-value)) of the difference in temporal correlations between each of the neuroprotected populations and the *mec-4* neurodegenerative mutants (*u231*) (Wilcoxon rank-sum test, FDR corrected). Indicated are P-values<0.01. *mec-4(u253)* n=80; *mec-4* (e1339) n=93; *mec-4 (u231)* n=93; *mec-4* (u231) + amiloride n=31, *mec-4* (u231);*crt-1*(bz29) n=58. *mec-4*:HisCl +histamine n=20; no HisCl transgene +histamine n=11.

Figure S5

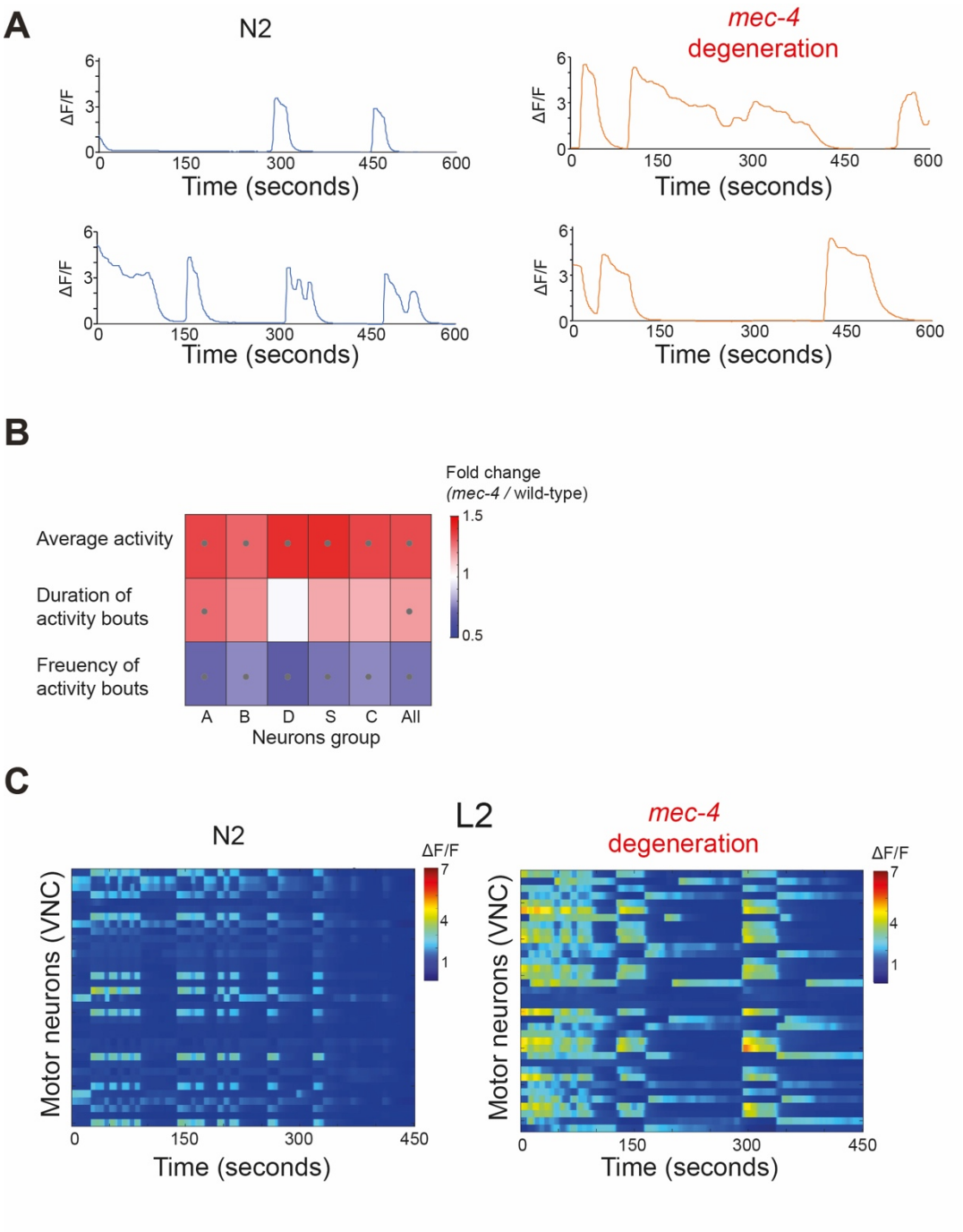
A
N2
mec-4
degeneration
ΔF/F
Time (seconds)
B
Fold change
(mec-4 / wild-type)
Average activity
Duration of
activity bouts
Freuency of
activity bouts
A B D S C All
Neurons group
C
N2
L2
mec-4
degeneration
Motor neurons (VNC)
Time (seconds)

Figure S5. Neuronal activity patterns in motor neurons in wild-type and TRN neurodegenerative mutants

(A) Examples of neuronal activity measurements over 10 minutes in single VNC motor neurons in L4 wild-type individuals (left) and *mec-4* neurodegenerative mutants *(u231)* in which the touch receptor neurons are degenerated (right) **(B)** Heatmap represents fold change difference in neuronal activity parameters of different groups of motor neurons between *mec-4* neurodegenerative mutants and wild-type individuals. Grey circles indicate P-value<0.05 (FDR corrected). N2: n=182,184,63,61,36 and *mec-4*: n=144,145,49,53,51 for the A,B,D,S,C motor neuronal groups, respectively.

(C) Heat maps represent spontaneous neuronal activity dynamics in motor neurons of a wild-type (left) and *mec-4* neurodegenerative mutant individual (right) over 15 minutes in the L2 stage. Color bar represents neuronal activity ($\Delta F/F$), smoothed using moving median (10 bins).